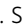

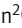






REPORT

Securin regulates the spatiotemporal dynamics of separase

Christopher G. Sorensen Turpin¹, Dillon Sloan², Marian LaForest³, Lindsey Klebanow⁴, Diana Mitchell⁵, Aaron F. Severson⁶, and Joshua N. Bembek¹

Separase regulates multiple aspects of the metaphase-to-anaphase transition. Separase cleaves cohesin to allow chromosome segregation and localizes to vesicles to promote exocytosis. The anaphase-promoting complex/cyclosome (APC/C) activates separase by ubiquitinating its inhibitory chaperone, securin, triggering its degradation. How this pathway controls the exocytic function of separase is unknown. During meiosis I, securin is degraded over several minutes, while separase rapidly relocalizes from kinetochore structures at the spindle and cortex to sites of action on chromosomes and vesicles at anaphase onset. The loss of cohesin coincides with the relocalization of separase to the chromosome midbivalent at anaphase onset. APC/C depletion prevents separase relocalization, while securin depletion causes precocious separase relocalization. Expression of non-degradable securin inhibits chromosome segregation, exocytosis, and separase localization to vesicles but not to the anaphase spindle. We conclude that APC/C-mediated securin degradation controls separase localization. This spatiotemporal regulation will impact the effective local concentration of separase for more precise targeting of substrates in anaphase.

Introduction

During mitosis, the metaphase-to-anaphase transition is regulated by the spindle assembly checkpoint (SAC) to ensure proper chromosome segregation (McAinsh and Kops, 2023; Musacchio, 2015). Once chromosomes are properly aligned on the spindle, SAC signaling is silenced and anaphase commences. Entry into anaphase requires the anaphase-promoting complex/cyclosome (APC/C), an E3 ubiquitin ligase (Alfieri et al., 2017). The APC/C is kept inactive by the SAC until anaphase onset when it ubiquitinates multiple substrates including securin, an inhibitory chaperone of separase (Watson et al., 2019). Separase is a protease that cleaves a subunit of cohesin, which links sister chromatids together, allowing anaphase onset (Uhlmann et al., 2000).

The SAC pathway also controls chromosome segregation during meiosis to form proper gametes (Gorbsky, 2015). Oocyte meiosis consists of two asymmetric divisions that generate a single large haploid gamete (Mogessie et al., 2018). In many species, oocytes are arrested in metaphase II prior to fertilization, which involves APC/C inhibition (Tunquist and Maller, 2003). Egg activation is triggered by fertilization, which

transforms the arrested oocyte into a rapidly dividing embryo. Egg activation events include the metaphase-to-anaphase transition and the exocytosis of cortical granule vesicles (Horner and Wolfner, 2008). Secreted cargo modifies the extracellular matrix of the oocyte to block polyspermy and protect the embryo (Liu, 2011; Liu et al., 2003; Wessel et al., 2001). Many fundamental cell cycle discoveries have been made by studying oocyte meiosis.

Caenorhabditis elegans is ideal for studying egg activation in vivo (Lui and Colaiácovo, 2013). Egg activation occurs during meiosis I in *C. elegans* oocytes (McCarter et al., 1999; McNally and McNally, 2005; Yang et al., 2005). Cortical granule exocytosis occurs during anaphase I, secreting eggshell material (Bembek et al., 2007; Olson et al., 2012). Importantly, separase localizes to cortical granules in anaphase I and promotes exocytosis, linking cell cycle regulation to vesicle trafficking (Bai and Bembek, 2017; Bembek et al., 2007, 2010; Mitchell et al., 2014; Richie et al., 2011). In human cells, securin is known as the pituitary tumor transforming gene, is overexpressed in cancers, and affects secretion (Donangelo et al., 2006; Heaney et al., 1999;

¹Department of Obstetrics and Gynecology, C.S. Mott Center for Human Growth and Development, Wayne State University School of Medicine, Detroit, MI, USA;

²Department of Biology, University of North Carolina, Chapel Hill, NC, USA; ³Columbia University, Herbert Irving Comprehensive Cancer Center, NYC, New York, NY, USA;

⁴Esko Bionics, San Rafael, CA, USA; ⁵Department of Biological Sciences, University of Idaho, Moscow, ID, USA; ⁶Center for Gene Regulation in Health and Disease and Department of Biological, Geological and Environmental Sciences, Cleveland State University, Cleveland, OH, USA.

Correspondence to Joshua N. Bembek: jbembek@wayne.edu.

© 2024 Sorensen Turpin et al. This article is distributed under the terms of an Attribution–Noncommercial–Share Alike–No Mirror Sites license for the first six months after the publication date (see <http://www.rupress.org/terms/>). After six months it is available under a Creative Commons License (Attribution–Noncommercial–Share Alike 4.0 International license, as described at <https://creativecommons.org/licenses/by-nc-sa/4.0/>).

Yu et al., 2000). Separase also regulates membrane trafficking in mammalian and plant cells (Bacac et al., 2011; Moschou et al., 2013), suggesting wide conservation of this role. How separase function during exocytosis is regulated by the SAC pathway is unknown.

The activation of separase after securin degradation has been extensively characterized using biochemical methods. However, the dynamics of separase localization are not well characterized. In yeast, securin is required for nuclear and spindle localization of separase (Agarwal and Cohen-Fix, 2002; Jensen et al., 2001). Mammalian separase localization is poorly characterized and has only been observed on chromosomes by staining overexpressed separase on chromosome spreads (Chestukhin et al., 2003; Shindo et al., 2012; Sun et al., 2009). Separase activity has been detected with biosensors at specific subcellular compartments (Agircan and Schiebel, 2014; MacKenzie et al., 2023; Monen et al., 2015; Nam and van Deursen, 2014; Rosen et al., 2019; Shindo et al., 2012; Weber et al., 2020). In *C. elegans* meiosis, separase localization has been well characterized, making it an ideal context to investigate how separase localization is regulated (Bembenek et al., 2007).

In *C. elegans* meiosis I, kinetochore cup structures form on holocentric homologous chromosomes (Fig. 1 A, Schvarzstein et al., 2010). Separase localizes to kinetochore cups in prometaphase I, appears at the midbivalent, where cohesin is found at anaphase onset, and then to “linker structures” between separating chromosomes in anaphase (Bembenek et al., 2007; Dumont et al., 2010; Muscat et al., 2015; Schvarzstein et al., 2010; Severson and Meyer, 2014). In the cortex, separase localizes to poorly characterized “linear elements” with kinetochore proteins during prometaphase I and then appears on cortical granules in anaphase I to promote exocytosis (Howe et al., 2001; Monen et al., 2005; Bai and Bembenek, 2017; Bembenek et al., 2007). How separase localization is regulated is not well understood.

We used live imaging to investigate the precise timing and regulation of separase dynamics. We find that while securin is degraded over several minutes, separase relocates seconds before cohesin is removed from chromosomes. Depletion of securin and APC/C affect separase localization on chromosomes and vesicles. We also characterize the phenotypes caused by non-degradable securin expression. Our findings suggest that APC/C and securin control both separase protease activity and its localization.

Results and discussion

Securin and separase dynamics during meiosis I

To characterize separase dynamics, we generated worms with endogenously tagged separase (SEP-1::GFP) or securin (IFY-1::GFP) with the chromosome marker H2B::mCherry. SEP-1::GFP localization is dynamic during meiosis I (Fig. 1, B–E). During prophase I, SEP-1::GFP is cytoplasmic and excluded from the nucleus (Fig. 1 B). Just before nuclear envelope breakdown (NEBD), SEP-1::GFP accumulates in the nucleus and becomes enriched on kinetochore cups (Fig. 1 C). Simultaneously, SEP-1::GFP appears on cytoplasmic linear element structures (Fig. 1,

C–D). In anaphase, SEP-1::GFP appears between chromosomes and is found on vesicles (Fig. 1 E). Therefore, separase moves from kinetochore structures to sites of action in anaphase.

We next investigated IFY-1::GFP localization during meiosis I. During prophase I, IFY-1::GFP is detected in the cytoplasm and is enriched in the nucleus while separase is excluded (Fig. 1 F). This nuclear pool of IFY-1::GFP is therefore likely not bound to separase. IFY-1::GFP colocalizes with SEP-1 at kinetochore cups and linear elements from NEBD through prometaphase I (Fig. 1, G, H, K, and L). Thus, separase is likely securin-bound and inactive when it localizes to kinetochore structures. IFY-1 signal begins to decline in the cytoplasm by late prometaphase I, ~3 min before anaphase onset, as previously described in worms (Fig. 1 N, Wang et al., 2013). By anaphase onset, weak IFY-1 signal remains at the midbivalent, which rapidly disappears (Fig. 1, I and N). We did not detect IFY-1 on vesicles at any timepoint (Fig. 1, F–I). Endogenously GFP tagged and multiple, independent transgenic lines show similar degradation curves regardless of expression level (Fig. S1, C and C'). In the cortex, IFY-1::GFP and SEP-1::mScarlet colocalize on linear elements until anaphase I when SEP-1::mScarlet localizes to vesicles and IFY-1::GFP is degraded (Fig. 1 O and Fig. S1 B). Therefore, SEP-1 colocalizes with IFY-1 at kinetochore structures until anaphase when IFY-1 is degraded and SEP-1 localizes to sites of action. These observations suggest that IFY-1 degradation may be required for SEP-1 to relocate in anaphase.

Rapid separase relocation at anaphase onset

To better define the dynamics of anaphase onset, we imaged separase, securin, and cohesin at the metaphase-to-anaphase transition with high spatiotemporal resolution. We observed a rapid separase relocation seconds before anaphase onset (Fig. 2, A–C and Video 1). During prometaphase I, separase localizes to kinetochore cups (Fig. 2 A) and is excluded from the midbivalent where the meiotic cohesin subunit, GFP::COH-3, localizes (Fig. 2, A and B). After spindle rotation, separase enriches at spindle poles ~30 s before anaphase I onset (Fig. 2, A and B; and Fig. S1 D, E, and F) and invades the midbivalent region within 10 s of anaphase onset, briefly colocalizing with GFP::COH-3 (Fig. 2, A and B; and Videos 1 and 2). When chromosomes move poleward, separase is highly enriched at the midbivalent and GFP::COH-3 is lost (Fig. 2, A and B; Fig. S2 A; and Fig. S1 D). Therefore, separase is spatially restricted from cohesin until seconds prior to anaphase onset.

We next wanted to determine the timing of securin degradation relative to separase relocation. To address this, we imaged GFP::IFY-1 with H2B::mCherry at high temporal resolution. During early metaphase I, the APC/C is required for meiotic spindle compaction, rotation, and translocation (Yang et al., 2003). During this time, spindle-associated GFP::IFY-1 gets redistributed and concentrated in the same pattern as separase, but the signal drops precipitously at spindle rotation, losing approximately a third of its average intensity by anaphase I onset (Fig. 2 C; Fig. 1, N and O; Fig. S1 A; and Video 1). When separase relocates to the midbivalent, securin levels rapidly decrease (Fig. 2 C; Fig. 1 O; and Fig. S1 A). At linear elements in the cortex, GFP::IFY-1 drops to near cytoplasmic levels before

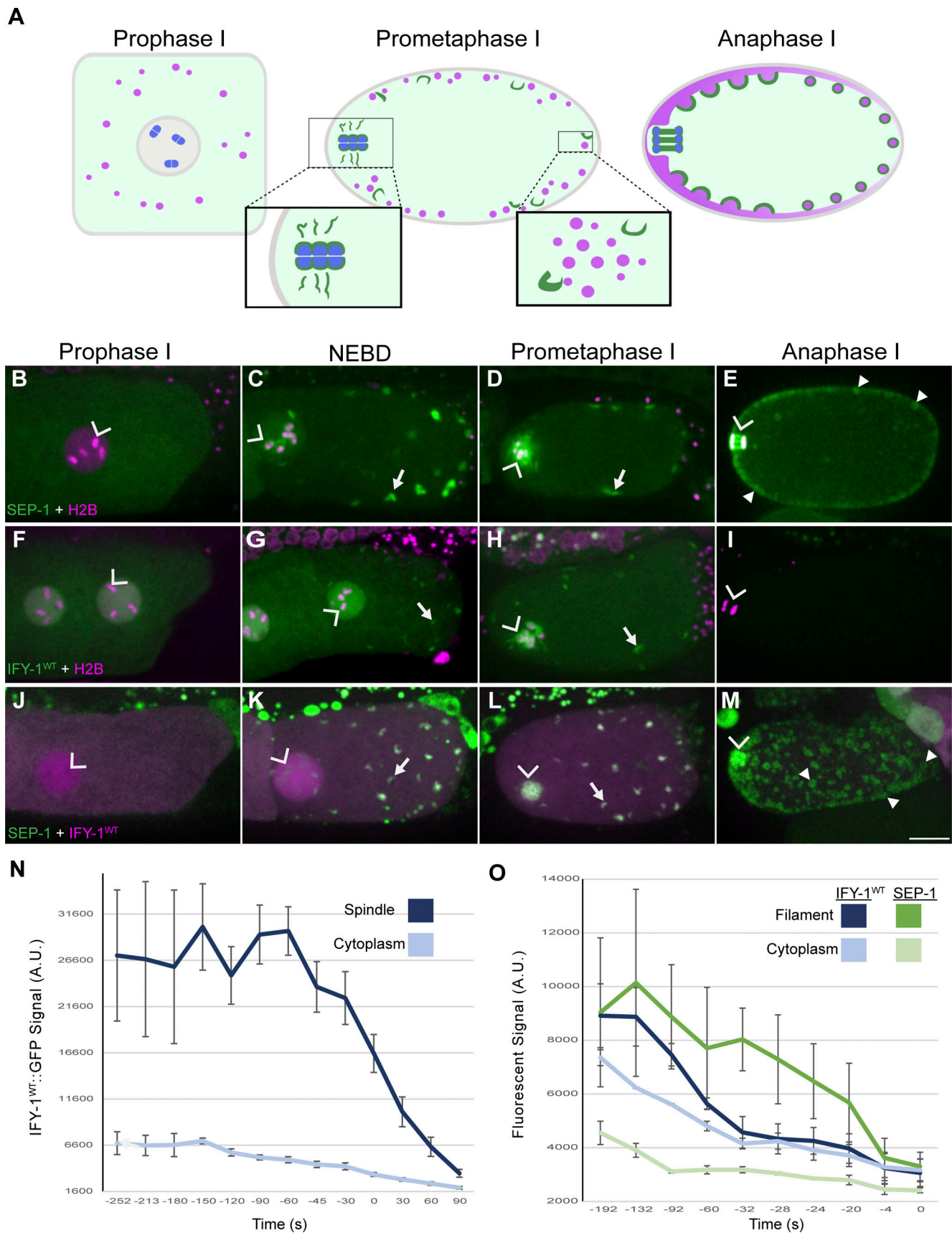


Figure 1. **Separase and securin dynamics in meiosis I.** (A) Diagram of meiosis I showing SEP-1 (green), chromosomes (blue), and cortical granules (magenta). Insets emphasize SEP-1 at the spindle (left) and cortex (right) during prometaphase I. (B–D) SEP-1::GFP (green) with H2B::mCherry (magenta) during meiosis I.

(B) During prophase I, SEP-1::GFP is cytoplasmic and excluded from the nucleus. **(C)** At NEBD, SEP-1::GFP accumulates on chromosomes in the nucleus (caret) and on cytoplasmic kinetochore linear elements in the cortex (white arrows), where it remains throughout prometaphase (D). **(E)** By mid-anaphase, separase localizes between separating chromosomes (caret) and vesicles (arrowheads). **(F–I)** IFY-1^{WT}::GFP (green) and H2B::mCherry (magenta) in meiosis I. **(F)** IFY-1^{WT}::GFP is present in both the cytoplasm and the nucleus in prophase. **(G and H)** IFY-1^{WT}::GFP displays identical localization patterns as separase at NEBD and through prometaphase I. **(I)** In anaphase I, IFY-1^{WT}::GFP is mostly degraded and is not observed on vesicles. **(J–M)** Endogenously tagged SEP-1::mScarlet (green) and IFY-1::GFP (magenta) colocalize at different stages as described above. **(N)** Quantification of IFY-1^{WT}::GFP spindle-associated and cytoplasmic signal showing rapid degradation ($t = 0$ is chromosome separation at anaphase onset). **(O)** Quantification of endogenously tagged SEP-1::mCherry and IFY-1^{WT}::GFP localized to linear elements and cytoplasm in the cortex, ($t = 0$ is separase localization to vesicles). Securin levels equilibrate with cytoplasmic signal before separase leaves linear elements and appears on vesicles. Scale bar: 10 μ m.

SEP-1::mScarlet relocates to vesicles (Fig. 1 O; Fig. S1 B; and Video 3). SEP-1::GFP is lost from linear elements and rapidly accumulates on cortical granules within 30 s after anaphase onset (Fig. 2 D and Video 3). Therefore, securin degradation rapidly occurs when separase relocates to sites of action at anaphase onset.

The APC/C-pathway controls SEP-1 localization in meiosis I

We next wanted to determine whether separase localization is controlled by APC/C-mediated securin degradation. Previously, cortical granule localization of separase was not observed after *ify-1* RNAi in *C. elegans* (Kimura and Kimura, 2012). We repeated this experiment to observe separase localization to chromosomes and vesicles. In control animals, the cortical granule cargo protein mCherry::CPG-2 is observed in vesicles in oocytes and embryos before anaphase I and is in the eggshell of older embryos (Fig. S2 A). In contrast to the previous report, we detected apparent SEP-1::GFP vesicle localization in multiple embryos in the uterus of *ify-1*(RNAi)-treated animals ($N = 16/30$ animals). To validate this result, we characterized separase localization in animals with different RNAi penetrance expressing SEP-1::GFP together with H2B::mCherry and mCherry::CPG-2. In mild phenotype cases (14–48 h of feeding RNAi), vesicle localization of separase is only observed in one or fewer embryos and mCherry::CPG-2 is observed in the eggshell of most embryos ($N = 31/101$ animals). Animals with an intermediate phenotype (16–39 h of feeding) had two to three unicellular embryos with SEP-1::GFP localized to mCherry::CPG-2 vesicles, while older embryos had gradually increasing eggshell mCherry::CPG-2 signal, suggesting reduced and delayed exocytosis ($N = 34/95$, Fig. S2 B). In severely affected animals (24–48 h of feeding RNAi), all embryos were unicellular and lacked extracellular mCherry::CPG-2 signal, with cortical granules trapped in the cytoplasm ($N = 31/61$, Fig. S2 C). Cortical granule localized SEP-1::GFP signal was reduced but still observed (Fig. S2 C). Therefore, securin depletion does not prevent separase localization to vesicles but inhibits exocytosis.

We next tested whether securin depletion, which should prematurely reduce securin levels, might cause premature separase relocation. To test this, we examined separase localization in embryos within the spermatheca, which are in early prometaphase I. In control animals, prometaphase I embryos have SEP-1::GFP at kinetochore cups (Fig. 3, A and A'; and Fig. S2, F and G) and linear elements ($N = 5/5$, Fig. 3 A'' and Fig. S2 A), with no vesicle localization. In intermediate and severe *ify-1*(RNAi) embryos, separase signal was reduced and mislocalized on chromosomes and could be observed between homologs where cohesin resides in embryos within the spermatheca ($N = 7/$

15 embryos, Fig. 3, B and B'; and Fig. S2 G). In addition, we observed SEP-1::GFP on cortical granules prematurely in *ify-1*(RNAi) embryos within the spermatheca ($N = 26/35$, Fig. 3 B''). Time-lapse recordings of oocytes from ovulation confirm that no vesicle signal is observed in control prometaphase I oocytes and embryos, but can be detected shortly after ovulation after *ify-1*(RNAi) treatment (Fig. S2, A' and B'). These results suggest that securin depletion causes premature relocation of separase.

We also depleted the APC/C, which is required for securin degradation, and examined separase localization. APC/C was also found to be required for separase to localize to vesicles (Kimura and Kimura, 2012). Severely affected *apc-2*(RNAi) embryos arrest in prometaphase I with mCherry::CPG-2 trapped in cortical granules (Fig. S2 D). As expected, *apc-2* RNAi blocked the degradation of IFY-1::GFP, which colocalized with SEP-1::mCherry on kinetochore structures in arrested embryos (Fig. S2 E). In *apc-2*(RNAi) embryos found in the spermatheca, SEP-1 is localized to kinetochore cups and linear elements like control embryos (Fig. 3, C–C''; and Fig. S2, D and E). Therefore, depletion of APC/C prevents securin degradation and separase relocation from kinetochore structures to sites of action.

Since separase relocates prematurely after securin depletion, we expected that it may also become proteolytically active prematurely. To test this, we examined embryos expressing GFP::COH-3 with chromosome marker H2B::mCherry (Fig. S3). Throughout prometaphase I, GFP::COH-3 appears as a crescent at the midbivalent, consistent with previous reports (McNally et al., 2022), which is likely a folded short arm axis of the homologous chromosomes (Fig. S3, B and B'). In WT embryos, GFP::COH-3 remains on chromosomes until seconds before chromosome segregation begins (Fig. S3 A and F). In prometaphase I embryos within the spermatheca, GFP::COH-3 signal remains high in control ($N = 10$) or *apc-2* RNAi ($N = 5$, Fig. S3, C, D, and G). In older embryos, COH-3 signal remained on chromosomes in arrested *apc-2*(RNAi) embryos but not in control embryos (Fig. S3, C and D). In contrast, prometaphase I *ify-1*(RNAi) embryos had a significant decrease in chromosomal GFP::COH-3 levels, consistent with prematurely active separase (Fig. S3, A, E, and F, $N = 13$). As expected, COH-3 persisted on chromosomes after anaphase onset in *sep-1*(RNAi) embryos (Fig. S3 A, $N = 7$ spindles). Therefore, securin depletion causes premature cohesin removal from chromosomes.

Non-degradable securin expression is dominant negative in *C. elegans*

APC/C and securin inactivation caused pleiotropic cell cycle defects. To directly test whether securin affects separase

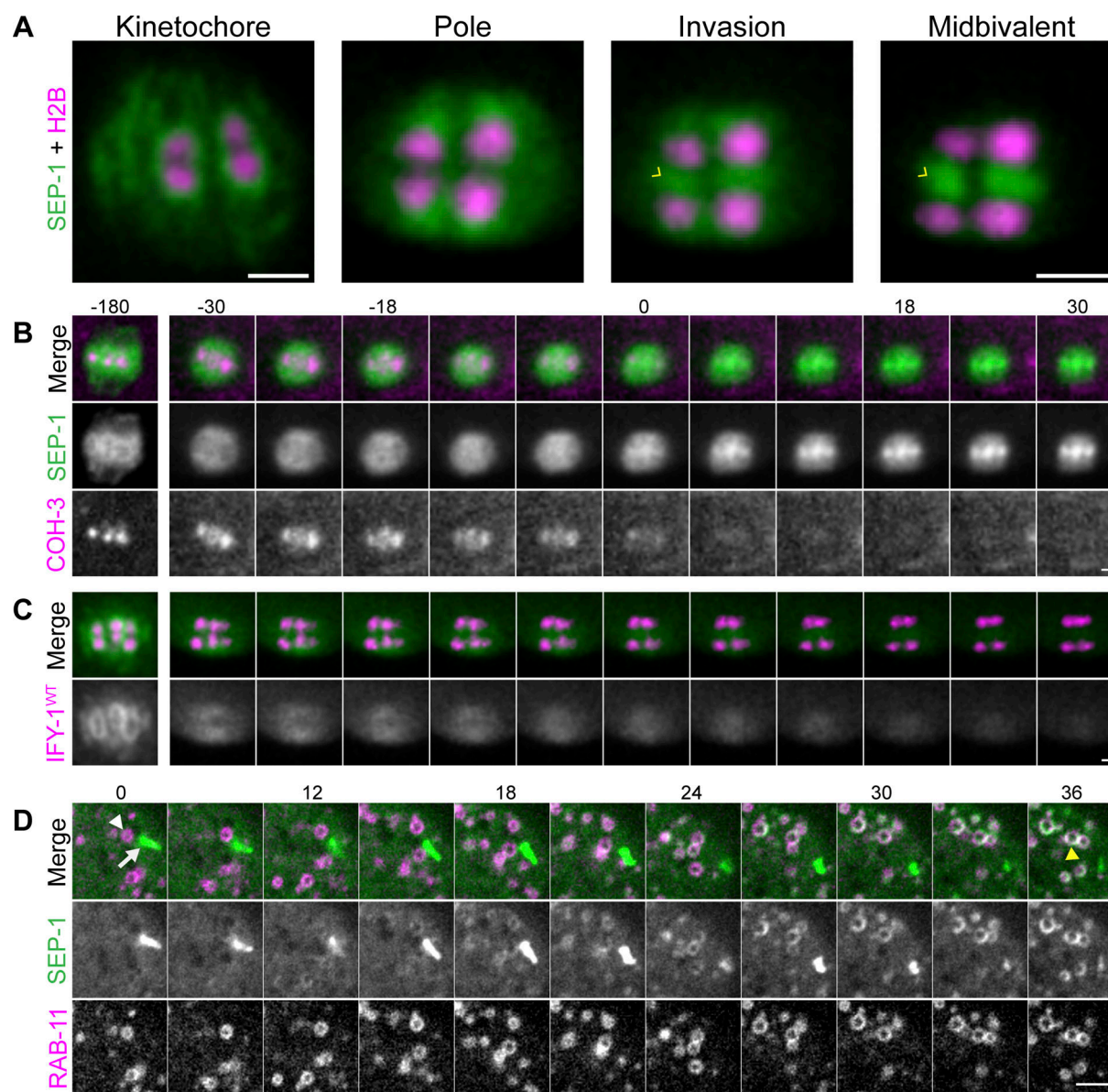


Figure 2. Dynamics of separase, securin, and cohesin at anaphase onset. (A) SEP-1::GFP (green) co-expressed with H2B::mCherry (magenta) at the spindle in meiosis I. In prometaphase I, spindle SEP-1::GFP localizes to kinetochore cups around the bivalents (kinetochore). Just before anaphase onset, SEP-1::GFP accumulates on spindle poles, then invades the midbivalent region (yellow caret), where it accumulates when chromosomes move apart. (B) Montage showing rapid SEP-1::mScarlet (green) relocalization to the midbivalent just before the abrupt loss of COH-3::GFP and the poleward movement of chromosomes (magenta, time in seconds relative to $t = 0$, anaphase onset). (C) Montage showing the dynamics of endogenous IFY-1^{WT}::GFP (green) co-expressed with chromosome marker H2B::mCherry (magenta) during the metaphase-to-anaphase I transition. IFY-1^{WT}::GFP signal is significantly reduced by anaphase onset. (D) In the cortex, SEP-1::GFP relocalizes from linear elements (white arrow) to cortical granules labeled with mScarlet::RAB-11.1 (arrowhead) by 30 s after anaphase onset. Scale bars: 2 μ m.

relocalization, we characterized a non-degradable mutant. In many systems, non-degradable securin expression causes cell division defects, (Cohen-Fix et al., 1996; Hagting et al., 2002; Herbert et al., 2003; Leismann et al., 2000; Zur and Brandeis, 2001), which has not been tested in worms. We developed methods for the expression of toxic transgenes in *C. elegans* using *gfp(RNAi)* and propagation of transgenes with female-biased promoters in the male germline to control expression (Mitchell et al., 2014). We made GFP::IFY-1 with mutations in the predicted N-terminal destruction box motif, required for APC/C

recognition (Kitagawa et al., 2002; Fig. 4 A). We generated transgenic lines with similar expression levels between wild type and mutant securin (Fig. S1, C and C') in a WT background. As expected, the expression of GFP::IFY-1^{DM}, but not GFP::IFY-1^{WT}, caused embryonic lethality (Fig. 4 B). The localization of GFP::IFY-1^{DM} was identical to wild type, except that it was not degraded in anaphase I (Fig. 4, C–F). During anaphase I, GFP::IFY-1^{DM} accumulated on the spindle, but was not observed on vesicles (Fig. 4 F). GFP::IFY-1^{DM} causes severe chromosome segregation and polar body extrusion defects ($N = 28/31$,

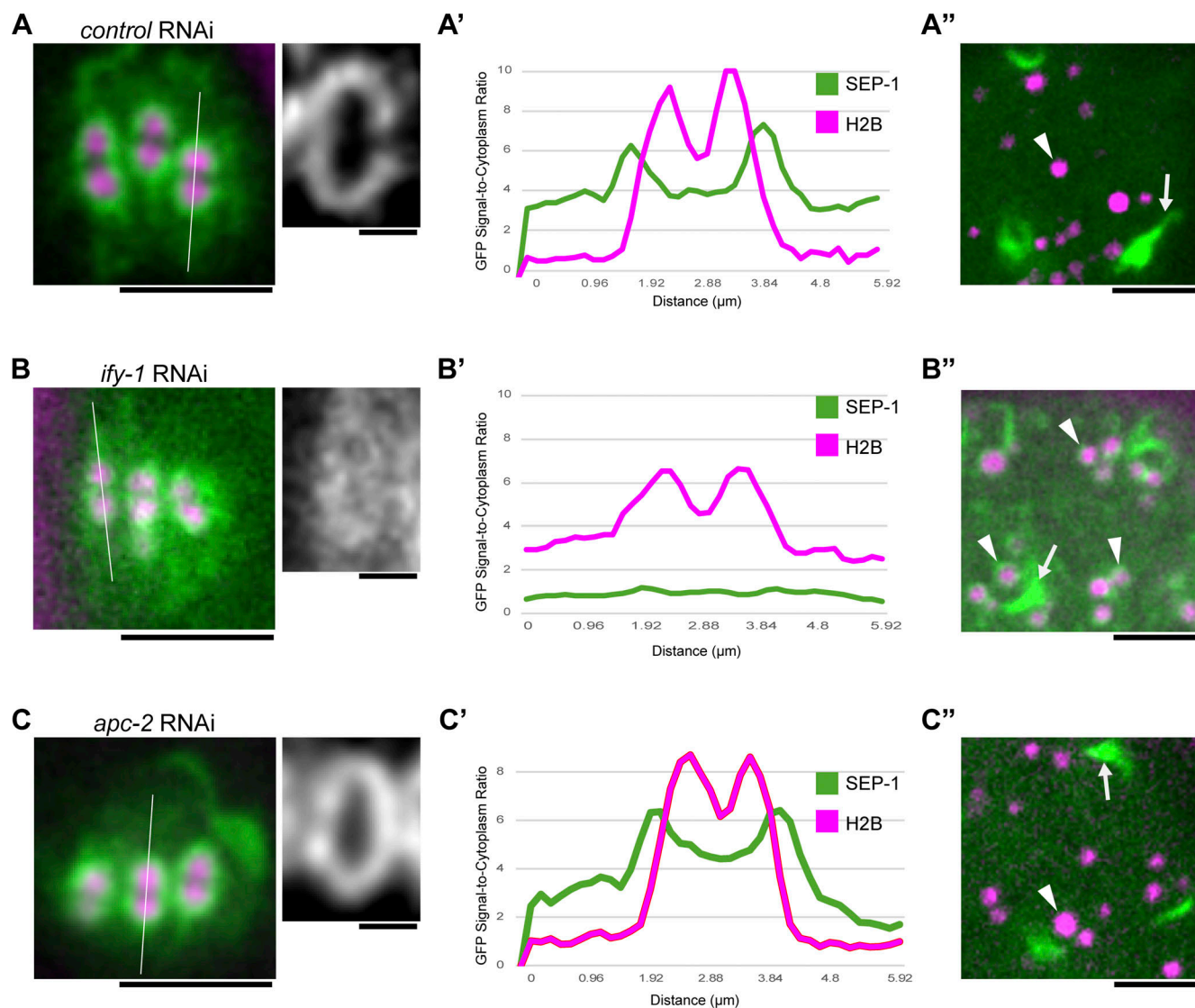


Figure 3. The APC/C and securin control SEP-1 localization in meiosis I. Prometaphase I embryos within the spermatheca expressing endogenously tagged SEP-1::GFP (green) with chromosome marker H2B::mCherry and cortical granule cargo protein mCherry::CPG-2 (magenta) in *control* (A–A''), *ify-1(RNAi)* (B–B''), or *apc-2(RNAi)* (C–C''). (A) In control embryos, SEP-1::GFP is localized to kinetochore cups and linear elements near the spindle (insets in A, B, and C show SEP-1::GFP on a bivalent in greyscale, white lines indicate the region used to generate a line scan in A', B', and C'). (A') Line scan showing the SEP-1::GFP and H2B::mCherry fluorescent profiles. (A'') In the cortex, SEP-1::GFP is localized to linear elements (arrow) but not vesicles (arrowhead). (B and B') Prometaphase I *ify-1(RNAi)* embryos have reduced SEP-1::GFP signal mislocalized at chromosomes, with some signal at the midbivalent. (B'') SEP-1::GFP precociously localizes to cortical granules (arrowheads) in addition to linear elements (arrow) after securin depletion. (C–C'') In *apc-2(RNAi)* prometaphase I embryos, SEP-1::GFP localization is normal on chromosomes and linear elements. Scale bars: 5 μ m, except the 1 μ m bars for insets found in A, B, and C.

Fig. 4 G). Older GFP::IFY-1^{DM} embryos shrink when dissected in high salt buffer ($N = 31/32$), which is never observed in wildtype ($N = 0/22$, Fig. 4 H), indicating an eggshell permeability defect. Therefore, GFP::IFY-1^{DM} is dominant negative and behaves as expected for a non-degradable mutant.

IFY-1^{DM} causes chromosome segregation defects during anaphase I

We examined chromosome segregation during meiosis I in embryos overexpressing GFP::IFY-1^{WT} or GFP::IFY-1^{DM} together with the chromosome marker H2B::mCherry (Fig. S4, A–D). Spindle rotation in GFP::IFY-1^{WT} embryos, which depends on

APC/C activity (Crowder et al., 2015; Ellefson and McNally, 2011), occurs 68 ± 7 s ($N = 6$) before anaphase onset. At anaphase onset, GFP::IFY-1^{WT} levels are rapidly decreasing and chromosomes move apart quickly (Fig. 2 C; and Fig. S4, A and C). In contrast, GFP::IFY-1^{DM} accumulates at the midbivalent 56 ± 6 s ($N = 16$) after spindle rotation (Fig. S4 B and Video 1). Chromosomes move apart 5 ± 2 s ($N = 6$) after midbivalent localization in GFP::IFY-1^{WT} embryos, but delay separation 115 ± 8.5 s ($N = 23$) after midbivalent localization in GFP::IFY-1^{DM} embryos (Fig. S4 A). After this extended delay, chromosomes move poleward at a significantly slower rate in the mutant relative to WT (Fig. S4, B and C). Chromosome segregation defects were observed in all

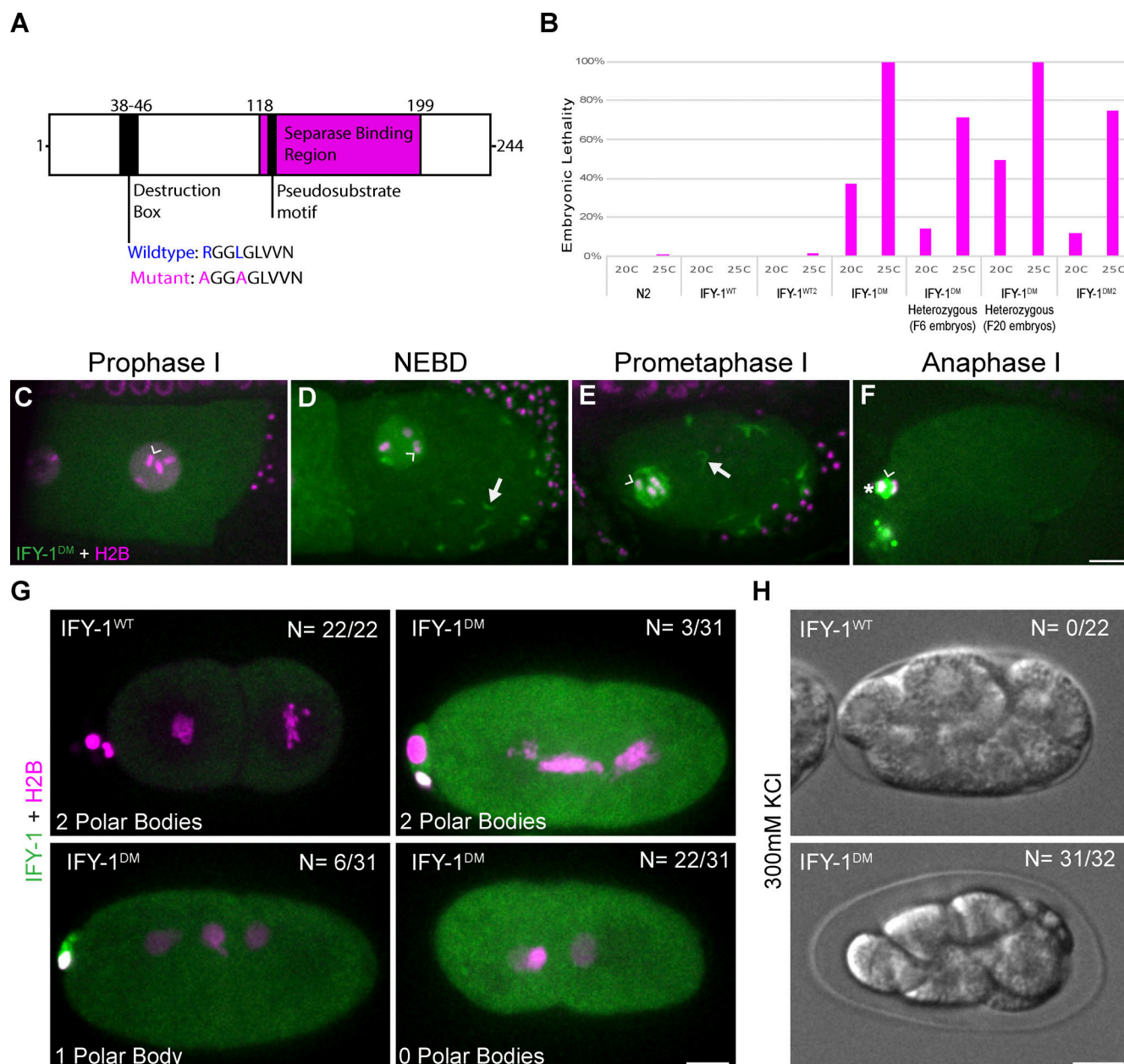


Figure 4. Generation and characterization of GFP::IFY-1^{DM} in *C. elegans*. (A) Schematic of IFY-1 indicating the APC/C recognition motif (destruction box) and mutated residues within the unstructured N-terminus. (B) Embryonic lethality of different GFP::IFY-1^{WT} and GFP::IFY-1^{DM} lines at 20°C and 25°C in homozygous or heterozygous animals. (C–F) IFY-1^{DM}::GFP (green) and H2B::mCherry (magenta) localization in meiosis I. GFP::IFY-1^{DM} has identical localization patterns as separase and wild type securin from prophase arrest through prometaphase I. (F) GFP::IFY-1^{DM} is not degraded in anaphase and accumulates on chromosomes (asterisk) and the anaphase I spindle (caret) but not on cortical granules. (G) In GFP::IFY-1^{WT}, two-celled embryos always have two small polar bodies (22/22 embryos) while GFP::IFY-1^{DM} embryos have high rates of polar body extrusion defects. (H) GFP::IFY-1^{WT} multicellular embryos are not permeable, while GFP::IFY-1^{DM} embryos all shrink in hyperosmotic solution, indicating permeability barrier defects. *N* = number of embryos scored. Scale bars: 10 μ m.

embryos expressing GFP::IFY-1^{DM} (*N* = 18/18, Fig. S4, B and D), but not in GFP::IFY-1^{WT} embryos (*N* = 5/5, Fig. S4, A and D). Finally, GFP::IFY-1^{DM} labeled structures in between chromosomes sometimes drift away from the spindle in late anaphase I (Fig. S4 B), but not in WT. Therefore, GFP::IFY-1^{DM} inhibits chromosome segregation and causes a novel delay between the midbivalent localization of securin and poleward chromosome movement.

IFY-1^{DM} blocks cortical granule exocytosis during anaphase I

We next investigated whether GFP::IFY-1^{DM} inhibits cortical granule exocytosis. We imaged embryos expressing GFP::IFY-1^{WT} or GFP::IFY-1^{DM} together with the cortical granule cargo protein, mCherry::CPG-2 during meiosis I (Fig. S4, E–K and Video 4). In WT embryos, cortical granule exocytosis occurs shortly after anaphase onset, releasing mCherry::CPG-2 into the eggshell (Fig. S4, E–H). In embryos expressing GFP::IFY-1^{DM},

most of the mCherry::CPG-2 labeled cortical granules do not undergo exocytosis during anaphase I (Fig. S4, E, G, I, and K). Therefore, GFP::IFY-1^{DM} expression causes a severe block of cortical granule exocytosis.

IFY-1^{DM} inhibits SEP-1 vesicle localization in anaphase I

Our results demonstrate that securin is a potent inhibitor of separase function during both chromosome segregation and exocytosis. While securin is known to inhibit separase protease activity, we wanted to investigate whether it also affects separase localization. Therefore, we examined endogenously tagged SEP-1::mScarlet in embryos expressing GFP::IFY-1^{WT} or GFP::IFY-1^{DM} during meiosis I (Fig. 5). From NEBD through prometaphase I, SEP-1::mScarlet colocalizes with GFP::IFY-1^{WT} and GFP::IFY-1^{DM} on kinetochore cups and linear elements (Fig. 5, A and B; and Video 5). After spindle rotation and shortening, SEP-1::mScarlet colocalizes with GFP::IFY-1^{WT} and GFP::IFY-1^{DM} at spindle poles, but GFP::IFY-1^{DM} accumulates at higher levels (Fig. 5, A and B). Separase relocates to the midbivalent in the presence of either the rapidly lost GFP::IFY-1^{WT} or the highly accumulated GFP::IFY-1^{DM} (Fig. 5, A and B). Therefore, expression of GFP::IFY-1^{DM} severely inhibits chromosome segregation without inhibiting the midbivalent or spindle localization of separase.

Next, we investigated whether securin affects separase localization to vesicles. We imaged SEP-1::mScarlet in the presence of overexpressed GFP::IFY-1^{WT} or GFP::IFY-1^{DM} (Fig. 5). Neither wild type nor mutant securin were detected on vesicles (Fig. 1, F–I and Fig. 4, C–F). SEP-1::mScarlet localized to vesicles normally in GFP::IFY-1^{WT} embryos ($N = 11/11$) but not in GFP::IFY-1^{DM} embryos ($N = 11/12$). To confirm vesicle localization, we co-expressed CAV-1::GFP (Sato et al., 2008) with GFP::IFY-1^{WT} or GFP::IFY-1^{DM} and examined SEP-1::mScarlet localization during anaphase I (Fig. 5, C–E). During prometaphase I, SEP-1 localizes to linear elements in GFP::IFY-1^{WT} or GFP::IFY-1^{DM} embryos (Fig. 5 C and Video 6). After anaphase I onset, SEP-1::mScarlet accumulates on vesicles in GFP::IFY-1^{WT} but not GFP::IFY-1^{DM} embryos (Fig. 5, C and D). In GFP::IFY-1^{WT} embryos, SEP-1::mScarlet rapidly accumulates on vesicles ~30 s after anaphase I onset, while 11/12 GFP::IFY-1^{DM} embryos showed weak and partial vesicle localization after a significant delay (207 ± 37 s). In GFP::IFY-1^{WT} embryos, SEP-1::mScarlet localized to 40 ± 1 vesicles ($N = 11$ embryos), while GFP::IFY-1^{DM} embryos had only 4 ± 1 SEP-1::mScarlet-positive vesicles ($N = 12$ embryos, Fig. 5 E). Therefore, GFP::IFY-1^{DM} interferes with cortical granule localization of SEP-1::mScarlet in anaphase I.

Perspectives and future directions

Previous studies have predominantly characterized separase regulation using in vitro assays (Rosen et al., 2019; Shindo et al., 2012; Yaakov et al., 2012). Separase is regulated by securin degradation (Cohen-Fix et al., 1996; Funabiki et al., 1996), autocleavage (Waizenegger et al., 2002), phosphorylation (Stemmann et al., 2001), isomerization (Hellmuth et al., 2015a), and CDK binding (Gorr et al., 2005; Yu et al., 2021). However, the localization of separase and its regulation at different subcellular locations has not been well characterized. Underscoring

the importance of separase localization, human cancer cells show aberrant separase nuclear localization (Meyer et al., 2009). Given that separase regulates centriole duplication (Tsou et al., 2009), anaphase spindle dynamics (Jensen et al., 2001), and vesicle exocytosis (Bembenek et al., 2007, 2010), different control mechanisms might regulate these cellular processes. Our results show that the spatiotemporal control of separase localization is critical for the proper regulation of anaphase events.

Securin is a pseudo-substrate inhibitory chaperone of separase (Boland et al., 2017; Hellmuth et al., 2014, 2015a, 2015b; Hornig et al., 2002; Viadiu et al., 2005). As such it serves multiple regulatory roles including (1) positively regulating the folding of separase (Hellmuth et al., 2015a); (2) enabling its spindle and nuclear localization (Hornig et al., 2002); (3) inhibiting its protease domain; and (4) acting as a competitive APC/C substrate for proper timing of events (Kamenz et al., 2015; Lu et al., 2014; Thomas et al., 2021). Securin loss could cause separase to become unfolded and inactive, mislocalized, and/or prematurely active based on its known functions. The reduction in separase signal we observed after securin depletion could reflect mislocalization and/or unstable separase. In addition, we observe that securin depletion causes premature relocalization of separase to sites of action and causes premature loss of cohesin from chromosomes. Therefore, part of the securin depletion phenotype is due to a premature activation of separase.

Interestingly, GFP::IFY-1^{DM} does not inhibit the midbivalent and spindle localization of separase but significantly interferes with vesicle localization. This indicates that securin degradation is necessary but not sufficient to regulate separase localization in anaphase. The colocalization of separase and securin with kinetochore proteins on chromosomes and linear elements suggests that kinetochore proteins bind to the separase/securin complex. Kinetochore proteins relocate to the midbivalent in anaphase (Dumont et al., 2010), where they may still be capable of binding separase and GFP::IFY-1^{DM}. However, linear elements disappear during anaphase, and kinetochore proteins are not known to localize to vesicles. Separase may bind directly to a substrate on vesicles, which would be inhibited by securin. We propose a model where separase is both kept inactive on kinetochore structures and away from substrates. APC/C-mediated securin degradation liberates separase protease activity and enables separase relocation to sites of action.

We suspect that the dynamic relocation of separase reflects an active transport mechanism. For example, spindle checkpoint inactivation at chromosomes involves dynein-mediated transport of proteins from the kinetochore to the centrosome (Griffis et al., 2007; Howell et al., 2001). In addition, APC/C regulates the microtubule motor activity required for spindle translocation (Yang et al., 2005). Finally, linear elements were shown to regulate cortical microtubules during polar body extrusion (Quiogue et al., 2023), which could also control separase localization. The spatiotemporal regulation of separase is an important facet of the metaphase-to-anaphase transition and may enable precise substrate cleavage by promoting a high local concentration of the enzyme near substrates.

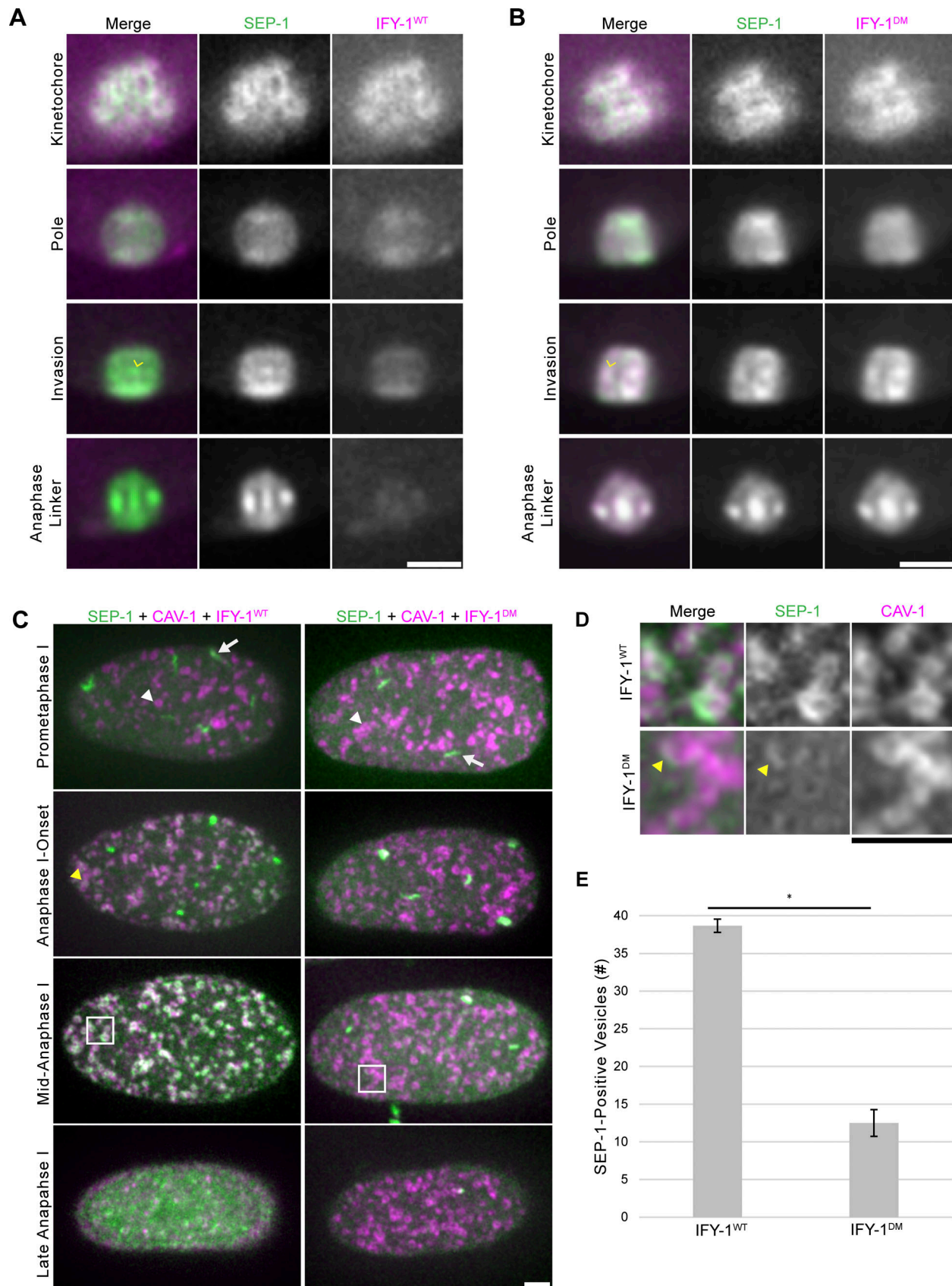


Figure 5. **Separase localization to vesicles is reduced by GFP::IFY-1^{DM}.** (A) Spindle localization of endogenously tagged SEP-1::mScarlet (green) co-expressed with GFP::IFY-1^{WT} (magenta). Securin is rapidly degraded while separase moves from kinetochores to the midbivalent (yellow arrowhead). (B) GFP::IFY-1^{DM} is stable in anaphase and colocalizes with separase in a similar pattern to wildtype. (C) Max projections of SEP-1::mScarlet (green) with vesicle marker

CAV-1::GFP (magenta) and either GFP::IFY-1^{WT} or GFP::IFY-1^{DM} (magenta). In prometaphase I, SEP-1 localizes to linear elements (white arrow) but not vesicles (white arrowheads) in both conditions. At anaphase I onset, SEP-1::mScarlet begins to enrich on vesicles (yellow arrowhead) in GFP::IFY-1^{WT} but not GFP::IFY-1^{DM} embryos. By mid-anaphase I, SEP-1::mScarlet is fully enriched on vesicles in GFP::IFY-1^{WT} embryos, but not in GFP::IFY-1^{DM} embryos. **(D)** Magnified images of SEP-1::mScarlet vesicle localization from the 5 μ m² regions indicated in C at mid-anaphase I in wildtype and mutant. SEP-1::mScarlet has only partial vesicle localization when GFP::IFY-1^{DM} is expressed (yellow arrowhead). **(E)** Quantification of vesicle-associated SEP-1::mScarlet signal in cortical planes at mid-anaphase I in GFP::IFY-1^{WT} (N = 11) and GFP::IFY-1^{DM} (N = 12) embryos. The asterisk denotes a statistically significant difference, P value <0.0001. Error bars represent the standard error of the mean. Scale bars: 5 μ m.

Materials and methods

C. elegans strains

Worm strains were maintained using standard protocols (Brenner, 1974; Mitchell et al., 2014). Some strains were obtained from the Caenorhabditis Genetics Center.

Generation of GFP::IFY-1^{DM} strains

The *ify-1* locus was PCR-amplified from genomic DNA to include restriction sites at the 5' (SpeI) and 3' end (MluI) for integration into the pJK3 plasmid, following established protocol (Gibson et al., 2009). The pJK3 plasmid allows N-terminal GFP fusion protein expression through the *pie-1* promoter. The highly conserved arginine (Arg38) and leucine (Leu41) within the conserved destruction box were mutagenized to alanine (RxxL → AxxA) using the Quickchange mutagenesis kit (Stratagene). Worms were transformed with the pJK3 plasmid carrying *gfp::ify-1^{dm}* using microparticle bombardment as previously described (Praitis et al., 2001).

Cloning and mutagenesis primers are listed below. Restriction sites are underlined and mutagenized residues are boldened.

ify-1 Forward cloning prime with SpeI site:

5'-CGCTCTAGAACTAGTATGGAGGATCTAAAC-3'

ify-1 Reverse cloning prime with MluI:

5'-ACGCGTTCACAGGGGAAGTTGGCTTCTTC-3'

ify-1^{dm} Forward destruction box mutagenesis primer:

5'-GGT**GCG**GGGCTGGTTGTAACTCGTCA-3'

ify-1^{dm} Reverse destruction box mutagenesis primer:

5'-AGTCGAGTTTACAACCAGCCC**CGC**ACCGCC**AGC**AGA AGG-3'.

Maintenance of GFP::IFY-1 RNAi stains

Multiple transformed worm lines were isolated and maintained using two methods we developed for the maintenance of worms harboring toxic transgenes (Mitchell et al., 2014). The first method exploits the transgenerational inheritance of siRNAs in *C. elegans*. Feeding animals *gfp* inhibits the expression of toxic GFP transgenes for an average of five generations in *C. elegans*. Using this first method, animals harboring *gfp::ify-1^{dm}* were grown on *gfp* RNAi plates for routine propagation. Animals carrying the GFP::IFY-1^{DM} transgene were then transferred onto OP50 plates and propagated for five generations. Fifth-generation hermaphrodites (F5) were selected, grown to adulthood, and their progeny were characterized. The second method involves mating male worms harboring our *pie-1* promoter-driven toxic transgenes with hermaphrodites. Using this method, we can indefinitely propagate *gfp::ify-1^{dm}* transgenes through the male germline because the *pie-1* promoter is not well expressed in the male germline. Male worms were mated with

hermaphrodites and their F1 hermaphrodite progeny were characterized.

Generation of endogenously tagged IFY-1^{WT}::GFP and SEP-1::mScarlet

CRISPR/Cas9 was used to generate endogenously tag the wild-type *ify-1* locus at the N-terminus with GFP and the wildtype *sep-1* locus at the C-terminus with mScarlet, as previously described (Paix et al., 2015). The repair templates were amplified from the pDD282 (plasmid # 66823; Addgene) and pMS050 (plasmid # 91826, gifts from Bob Goldstein; Addgene). The primer sequences and repair templates used are listed below. Underlined amino acids denote flexible linker sequences.

ify-1::gfp Forward: 5'-ACGACCTCCTCGCCGAAGAAGCCAACC TTCCCTGGGAGCATCGGGAGCCGGAGCATCGGGAGCC-3'

ify-1::gfp Reverse: 5'-AAACAGGTAGAAGAGGCTGACGTCGTG GGAAATCACTTGTAGAGCTCGTCCATTC-3'.

The *ify-1::gfp* guide RNA: 5'-GACGUCGUGGGAAAUCACAGG UUUUAGAGCUAUGCUGUUUUG-3'

sep-1::gfp Forward:

5'-CAAGTGCCCGAACTCCATCAAGATCCCGAAATTTGGGA GCATCGGGAGCCTCAGGAGCATCGATGGTCTCCAAGGG-3'

sep-1::gfp Reverse:

5'-ACGATCCTTAAGATCCTTCGGGTCAGATTATATTACTTG TAGAGCTCGTCCATTC-3'.

The *sep-1::gfp* guide RNA:

5'-CAGAUUAUAUUACAAAUUUCGUUUUAGAGCUAUGCUGUUUUG-3'.

Creation of ySi12 *Ppie-1::GFP::coh-3*

The *coh-3* coding sequence and 3' UTR were amplified from fosmid WRM068bC06 (Geneservice Ltd.) by PCR with primers AFS357 (5'-GGGGACAGCTTTCTTGACAAAAGTGGctATGGTGAT AAGCATCGATGTACC-3') and AFS358 (5'-GGGGACAACCTT GTATAATAAAGTTGGCGCCTTTAAAGCTACCTGTAAC-3'). The PCR product was cloned into pDONRP2R-P3 via a Gateway BP Cloning reaction (Thermo Fisher Scientific). A single missense mutation identified in the resulting plasmid and the parental fosmid was repaired by site-directed mutagenesis using primers AFS436 (5'-TGAGTACTGAGAAGTATGGTGTTC-3') and AFS437 (5'-AGTTGCTCGACTTCTTCGTAC-3'), yielding the error-free entry clone pAS139. pAS139 was used in a multisite Gateway LR reaction together with entry plasmids pCG142 (*pie-1* intron:*pie-1* promoter in PDONRP4PIR) and pCM1.53 (GFP with worm codon bias and synthetic introns in pDONR201) (plasmids # 17246 and # 17250, gifts from Geraldine Seydoux; Addgene) and destination vector pCFJ150 - pDESTttTi5605[R4-R3] (plasmid # 19329, gift from Erik Jorgensen; Addgene). The resulting targeting vector, pAS142, was inserted into the *ttTi5605*

Mos1 transposon site in strain EG4322 by MosSCI to create the single-copy integrated transgene γ SiI2[*Ppie-1::GFP::coh-3*] (Frøkjær-Jensen et al., 2008; Merritt et al., 2008). γ SiI2 encodes a functional GFP::COH-3 fusion since it increases the embryonic viability of *coh-4(tm1857) coh-3(gkl12)* double mutants from 3.1% ($n = 1246$) to 91.8% ($n = 1522$) and decreases male production from 36% ($n = 25$) to 3.8% ($n = 1316$). The low number of *coh-4 coh-3* animals scored for male production is due to the low rate of survival of these worms to adulthood; this phenotype is also rescued by the γ SiI2 transgene.

RNAi treatments

Feeding RNAi was conducted as previously described using HT115 bacteria harboring the L4440 plasmid (Grishok et al., 2005). For *apc-2* and *ify-1* feeding RNAi, L4 hermaphrodites from WH416, JAB20, and JAB258 (Table S1) lines were plated onto the induced RNAi bacterial strains at 20°C or 25°C, and phenotype severity and penetrance were assessed after 14–48 h of treatment.

Characterization of GFP::IFY-1^{DM} Lines

IFY-1 degradation curve and spindle curve

Degradation curve values are expressed as ratios reflecting the mean cytoplasmic GFP intensity in the newly fertilized oocyte relative to mean cytoplasmic GFP values in the –1 oocyte over time. Values for each timepoint correspond to an average of at least five independent movies for each IFY-1^{WT} or IFY-1^{DM} strain.

Embryonic lethality

Lethality assays were performed as previously described (Mitchell et al., 2014). Lines expressing GFP::IFY-1^{WT} or GFP::IFY-1^{DM} were grown under identical conditions at 20°C or 25°C and embryo lethality was quantified. Lethality rates reflect the pooled average of embryonic lethality for each strain and condition after 24 h.

Polar body extrusion rate

The polar body extrusion assay was performed using embryos dissected from mothers homozygous for H2B::mCherry and GFP::IFY-1^{WT} or GFP::IFY-1^{DM} five generations removed from *gfp* RNAi feeding. We quantified two cell-stage embryos to allow for the completion of meiosis and quantify polar bodies before the second polar body is internalized and degraded in older embryos (Fazeli et al., 2018).

Embryonic osmotic sensitivity

The osmotic sensitivity assay was performed by dissecting wildtype (N2) or homozygous GFP::IFY-1^{DM} mutant embryos in a hypertonic solution of 300 mM KCl, as described (Knight et al., 2012). Animals were five generations removed from *gfp* RNAi feeding. Embryos were scored for normal appearance or obvious shrinkage.

Live cell imaging

Live cell imaging data was collected using spinning disk confocal systems using either an inverted Nikon Eclipse microscope with

a 60× 1.40NA objective, a CSU-22 spinning disc system, and a Photometrics EM-CCD camera from Visitech International operated by MetaMorph software (Molecular Devices), or an inverted Nikon Eclipse Ti2-E with a 60× 1.42NA objective and 100× 1.45 NA objective, a CSU-X1 spinning disc system, and Andor iXon Life camera operated by NIS-Elements software (Nikon). Unless otherwise mentioned, live cell imaging was conducted at room temperature which was ~20°C. Anaphase onset was determined using the movement of chromosomes or the presence of separase and/or securin at the midbivalent. Image analysis and manipulation were performed in Fiji (National Institutes of Health), Adobe Photoshop, and Adobe Illustrator (Adobe).

In utero live cell imaging

We used two immobilization methods to mount animals to image oocytes and embryos. The first method was an optimized nanoparticle-mediated immobilization technique based on a previously described protocol (Kim et al., 2013). This first strategy was used for Fig. 1, B–M; Fig. 3, A–C''; Fig. 4, C–F; Fig. S1, C, E, and F; Fig. S2, C–G; and Fig. S3, A–E. We also used a chemical immobilization method by mounting worms in an M9 solution containing 5 mM levamisole on a 2% agarose pad following standard protocol (Bai and Bembenek, 2017; Bembenek et al., 2007; Mitchell et al., 2014). We used this second strategy for initially documenting *control*, *apc-2*, and *ify-1* RNAi phenotypes, and for data presented in Fig. 3, A–C'' and Fig. S3, A–E.

Time-lapse imaging of meiosis I ex utero

Before eggshell formation, meiotic embryos are especially fragile to osmotic and mechanical perturbations (Stein and Golden, 2018). To minimize perturbations ex utero, meiotic embryos were dissected from hermaphrodites in blastomere culture media using the hanging drop mounting technique (Edgar and Goldstein, 2012). Parental carcasses were removed from the media along with bacteria to prevent toxic effects associated with their presence when left in the media (Bai and Bembenek, 2017; Bembenek et al., 2007; Mitchell et al., 2014). Cortical granules have weak autofluorescence under 488-nm illumination that is quickly bleached after 25 exposures with standardized settings. The autofluorescent signal can be visually distinguished because it fills the vesicle, while our GFP fusion proteins appear to coat the membrane of the vesicle. Therefore, in conditions with weak GFP signal, we systematically performed an autofluorescence prebleach exposure before imaging GFP localization. For all ex utero imaging, L4 hermaphrodites were shifted from 20°C to 25°C for 18–24 h before imaging at either room temperature or 25°C. This approach was used for acquiring data for Fig. 1, E, N, and O; Fig. 2, A–D; Fig. 4 G; Fig. S1, A, B, and D; Fig. S2, A and B; Fig. S4, A, B, and F–K; and Videos 1, 2, 3, 4, 5, and 6.

Quantifications

Fluorescence

Fluorescent values for degradation curves in Fig. 1 were acquired from single plane, *ex utero* movies of meiosis I embryos at approximately the same z-depth and using the same acquisition settings. The values represent the binned average signal from

two to five independent movies, found in a three-pixel diameter circle at the spindle, filament, and cytoplasm. The values for each movie and each timepoint at these regions of interest are averages of between one and five independent measurements per movie minus the average background signal.

Fluorescent values for the securin degradation curves in Fig. S1 were acquired from single-plane, in utero movies of meiosis I. Worm age, imaging conditions (room temperature), and acquisition settings were identical for all data acquisition. Values represent the binned average of at least two to four independent movies, found in a 10-pixel diameter circle in the bulk cytoplasm. The values for each movie and each timepoint are averages of three independent cytoplasmic measurements minus the average background signal.

Quantification of prometaphase I GFP::COH-3 levels in Fig. S3 F were made from single-plane, in utero, movies after RNAi treatments (*control* and *ify-1*). One to three 3-pixel diameter circle region of GFP::COH-3 and H2B::mCherry signal were measured and averaged, subtracting the average background signal within a three-pixel diameter circle and expressed as a ratio. Curves reflect COH-3 levels over time for a single embryo for each condition.

Quantification of prometaphase I GFP::COH-3 levels in Fig. S3 G were made from single-plane, in utero, movies after RNAi treatments (*control*, *apc-2*, and *ify-1*). The calculated signal ratio corresponds to the midbivalent signal of the -1 oocyte to a prometaphase I oocyte in the spermatheca acquired in the same plane in a single image. A three-pixel diameter circle region of GFP::COH-3 signal was measured, subtracting the average background signal within a three-pixel diameter circle. Each condition is an average of 5–13 independent worms.

Quantification of SEP-1::GFP kinetochore-to-cytoplasm ratios in Fig. S2, F and G were made from single-plane, in utero, movies and images after RNAi treatments (*control*, *apc-2*, and *ify-1*). Specifically for S2 F and SEP-1::GFP kinetochore values, two to five independent measurements were averaged from pixel values contained within a two-pixel diameter circle and subtracted from the average value of background from a 20-pixel diameter circle. For SEP-1::GFP cytoplasm values, a single measurement of a 20-pixel diameter circle was made with the background subtracted from a single measurement from the same-sized circle. Specifically for Fig. S2 G, we chose to analyze ideal cross sections of bivalent pairs per previously described parameters (Danlasky et al., 2020). To calculate SEP-1::GFP at the kinetochore and within the midbivalent region, GFP values were averages from three, single-pixel measurements from each structure on a per-bivalent basis, and the average background from GFP values within a 20-pixel diameter circle were subtracted out.

GFP::IFY-1^{DM} reduction of separase vesicle localization (Fig. 5 D)

We were unable to generate viable animals with homozygous GFP::IFY-1^{DM} and homozygous SEP-1::mScarlet, but heterozygous GFP::IFY-1^{DM} was viable when combined with heterozygous SEP-1::mScarlet. Extensive troubleshooting was taken to avoid phototoxicity and photobleaching, while simultaneously being able to evaluate SEP-1 vesicle localization. To time

anaphase I onset, we imaged GFP alone using a single plane until GFP::IFY-1^{DM} was detected at the midbivalent. We then quickly switched to multiplane imaging (5 μ m steps \times 3 planes) acquired every 45–120 s so that we could capture cortical planes over the course of an extended anaphase. Wildtype data was acquired only using multiplane *ex utero* imaging because embryos were not sensitive to phototoxicity or photobleaching problems within the normal duration of anaphase I. Quantification of SEP-1::GFP signal at vesicle structures was performed on movies with z planes that had a similar circumference to ensure a similar region of the cortex was quantified.

Line scans (Fig. 3)

To quantitatively assess separase kinetochore localization after RNAi treatments, a one-pixel-wide line scan was generated from representative images along the prometaphase I spindle axis through a clearly resolved cross section of a homologous chromosome pair. Fluorescent intensities were generated using Fiji for both separase and H2B signal with the average background subtracted out. Average bulk cytoplasm was determined, with average background subtracted out. Background corrected values for the line scan were divided by background corrected values for the bulk cytoplasm for normalization.

Statistics

Calculations for P values were done in Microsoft Excel using Student's *t* test (two-tailed, assuming unequal variance) to determine statistical significance.

Online supplemental material

Fig. S1 shows separase and securin localization during meiosis I, quantification of securin expression lines, and separase colocalization with spindle markers (related to Figs. 1 and Fig. 2). Fig. S2 shows in utero images of separase localization in different conditions (related to Fig. 3). Fig. S3 describes cohesin dynamics, morphology, and regulation during meiosis I (related to Figs. 2 and 3). Fig. S4 documents the dominant negative phenotypes caused by the expression of non-degradable securin (related to Figs. 4 and 5). Table S1 lists the *C. elegans* strains used in this study. Video 1 shows the dynamics of separase, cohesin, and securin on chromosomes during the metaphase-to-anaphase transition (related to Figs. 1 and 2). Video 2 shows separase dynamics relative to chromosomes, cohesin, and securin at anaphase I onset (related to Fig. 2). Video 3 shows securin and separase in the cortex during metaphase–anaphase I (related to Fig. 2). Video 4 shows cortical granule exocytosis during meiosis I in embryos expressing WT or non-degradable securin (related to Figs. 4 and 5). Video 5 shows that non-degradable securin does not affect separase relocalization to the midbivalent in anaphase I (related to Figs. 4 and 5). Video 6 shows that non-degradable securin prevents separase from localizing to cortical granules during anaphase I (Related to Figs. 4 and 5).

Data availability

The data are available from the corresponding author upon reasonable request.

Acknowledgments

We thank Julie Ahringer, Arshad Desai, Barth Grant, Tony Hyman, Karen Oegema, Martha Soto, and Asako Sugimoto for sharing strains and members of the Bembenek laboratory for comments and support.

CGC and Wormbase provided *C. elegans* strains and information, funded by the National Institutes of Health (NIH) (P40 OD010440) and the National Human Genome Research Institute (U41 HG002223). Funding was provided by the NIH grants R15 GM143731 to A.F. Severson and R01 GM114471 to J.N. Bembenek.

Author contributions: C.G. Sorensen Turpin: Conceptualization, Data curation, Formal analysis, Investigation, Methodology, Validation, Visualization, Writing - original draft, Writing - review & editing, D. Sloan: Resources, M. LaForest: Data curation, Investigation, L. Klebanow: Investigation, D. Mitchell: Investigation, Methodology, Resources, Writing - review & editing, A.F. Severson: Conceptualization, Resources, Writing - review & editing, J.N. Bembenek: Conceptualization, Data curation, Formal analysis, Funding acquisition, Methodology, Project administration, Resources, Supervision, Validation, Visualization, Writing - original draft, Writing - review & editing.

Disclosures: The authors declare no competing interests exist.

Submitted: 20 December 2023

Revised: 25 July 2024

Accepted: 28 October 2024

References

- Agarwal, R., and O. Cohen-Fix. 2002. Phosphorylation of the mitotic regulator Pds1/securin by Cdc28 is required for efficient nuclear localization of Esp1/separase. *Genes Dev.* 16:1371–1382. <https://doi.org/10.1101/gad.971402>
- Agircan, F.G., and E. Schiebel. 2014. Sensors at centrosomes reveal determinants of local separase activity. *PLoS Genet.* 10:e1004672. <https://doi.org/10.1371/journal.pgen.1004672>
- Alfieri, C., S. Zhang, and D. Barford. 2017. Visualizing the complex functions and mechanisms of the anaphase promoting complex/cyclosome (APC/C). *Open Biol.* 7:170204. <https://doi.org/10.1098/rsob.170204>
- Bacac, M., C. Fusco, A. Planche, J. Santodomingo, N. Demareux, R. Leemann-Zakaryan, P. Provero, and I. Stamenkovic. 2011. Securin and separase modulate membrane traffic by affecting endosomal acidification. *Traffic*. 12:615–626. <https://doi.org/10.1111/j.1600-0854.2011.01169.x>
- Bai, X., and J.N. Bembenek. 2017. Protease dead separase inhibits chromosome segregation and RAB-11 vesicle trafficking. *Cell Cycle*. 16:1902–1917. <https://doi.org/10.1080/15384101.2017.1363936>
- Bembenek, J.N., C.T. Richie, J.M. Squirrell, J.M. Campbell, K.W. Eliceiri, D. Poteryaev, A. Spang, A. Golden, and J.G. White. 2007. Cortical granule exocytosis in *C. elegans* is regulated by cell cycle components including separase. *Development*. 134:3837–3848. <https://doi.org/10.1242/dev.011361>
- Bembenek, J.N., J.G. White, and Y. Zheng. 2010. A role for separase in the regulation of RAB-11-positive vesicles at the cleavage furrow and mid-body. *Curr. Biol.* 20:259–264. <https://doi.org/10.1016/j.cub.2009.12.045>
- Boland, A., T.G. Martin, Z. Zhang, J. Yang, X.C. Bai, L. Chang, S.H.W. Scheres, and D. Barford. 2017. Cryo-EM structure of a metazoan separase-securin complex at near-atomic resolution. *Nat. Struct. Mol. Biol.* 24: 414–418. <https://doi.org/10.1038/nsmb.3386>
- Brenner, S. 1974. The genetics of *Caenorhabditis elegans*. *Genetics*. 77:71–94. <https://doi.org/10.1093/genetics/77.1.71>
- Chestukhin, A., C. Pfeffer, S. Milligan, J.A. DeCaprio, and D. Pellman. 2003. Processing, localization, and requirement of human separase for normal anaphase progression. *Proc. Natl. Acad. Sci. USA*. 100:4574–4579. <https://doi.org/10.1073/pnas.0730733100>
- Cohen-Fix, O., J.M. Peters, M.W. Kirschner, and D. Koshland. 1996. Anaphase initiation in *Saccharomyces cerevisiae* is controlled by the APC-dependent degradation of the anaphase inhibitor Pds1p. *Genes Dev.* 10: 3081–3093. <https://doi.org/10.1101/gad.10.24.3081>
- Crowder, M.E., J.R. Flynn, K.P. McNally, D.B. Cortes, K.L. Price, P.A. Kuehnert, M.T. Panzica, A. Andaya, J.A. Leary, and F.J. McNally. 2015. Dynactin-dependent cortical dynein and spherical spindle shape correlate temporally with meiotic spindle rotation in *Caenorhabditis elegans*. *Mol. Biol. Cell*. 26:3030–3046. <https://doi.org/10.1091/mbc.E15-05-0290>
- Danlasky, B.M., M.T. Panzica, K.P. McNally, E. Vargas, C. Bailey, W. Li, T. Gong, E.S. Fishman, X. Jiang, and F.J. McNally. 2020. Evidence for anaphase pulling forces during *C. elegans* meiosis. *J. Cell Biol.* 219:12. <https://doi.org/10.1083/jcb.202005179>
- Donangelo, I., S. Gutman, E. Horvath, K. Kovacs, K. Wawrowsky, M. Mount, and S. Melmed. 2006. Pituitary tumor transforming gene overexpression facilitates pituitary tumor development. *Endocrinology*. 147: 4781–4791. <https://doi.org/10.1210/en.2006-0544>
- Dumont, J., K. Oegema, and A. Desai. 2010. A kinetochore-independent mechanism drives anaphase chromosome separation during acen-trosomal meiosis. *Nat. Cell Biol.* 12:894–901. <https://doi.org/10.1038/ncb2093>
- Edgar, L.G., and B. Goldstein. 2012. Culture and manipulation of embryonic cells. *Methods Cell Biol.* 107:151–175. <https://doi.org/10.1016/B978-0-12-394620-1.00005-9>
- Ellefson, M.L., and F.J. McNally. 2011. CDK-1 inhibits meiotic spindle shortening and dynein-dependent spindle rotation in *C. elegans*. *J. Cell Biol.* 193:1229–1244. <https://doi.org/10.1083/jcb.201104008>
- Fazeli, G., M. Stetter, J.N. Lisack, and A.M. Wehman. 2018. *C. elegans* blastomeres clear the corpse of the second polar body by LC3-associated phagocytosis. *Cell Rep.* 23:2070–2082. <https://doi.org/10.1016/j.celrep.2018.04.043>
- Frøkjær-Jensen, C., M.W. Davis, C.E. Hopkins, B.J. Newman, J.M. Thummel, S.-P. Olesen, M. Grunnet, and E.M. Jorgensen. 2008. Single-copy insertion of transgenes in *Caenorhabditis elegans*. *Nat. Genet.* 40: 1375–1383. <https://doi.org/10.1038/ng.248>
- Funabiki, H., K. Kumada, and M. Yanagida. 1996. Fission yeast Cut1 and Cut2 are essential for sister chromatid separation, concentrate along the metaphase spindle and form large complexes. *EMBO J.* 15:6617–6628. <https://doi.org/10.1002/j.1460-2075.1996.tb01052.x>
- Gibson, D.G., L. Young, R.-Y. Chuang, J.C. Venter, C.A. Hutchison III, and H.O. Smith. 2009. Enzymatic assembly of DNA molecules up to several hundred kilobases. *Nat. Methods*. 6:343–345. <https://doi.org/10.1038/nmeth.1318>
- Gorbsky, G.J. 2015. The spindle checkpoint and chromosome segregation in meiosis. *FEBS J.* 282:2471–2487. <https://doi.org/10.1111/febs.13166>
- Gorr, I.H., D. Boos, and O. Stemmann. 2005. Mutual inhibition of separase and Cdk1 by two-step complex formation. *Mol. Cell*. 19:135–141. <https://doi.org/10.1016/j.molcel.2005.05.022>
- Griffis, E.R., N. Stuurman, and R.D. Vale. 2007. Spindly, a novel protein essential for silencing the spindle assembly checkpoint, recruits dynein to the kinetochore. *J. Cell Biol.* 177:1005–1015. <https://doi.org/10.1083/jcb.200702062>
- Grishok, A., J.L. Sinsky, and P.A. Sharp. 2005. Transcriptional silencing of a transgene by RNAi in the soma of *C. elegans*. *Genes Dev.* 19:683–696. <https://doi.org/10.1101/gad.1247705>
- Hagting, A., N. Den Elzen, H.C. Vodermaier, I.C. Waizenegger, J.-M. Peters, and J. Pines. 2002. Human securin proteolysis is controlled by the spindle checkpoint and reveals when the APC/C switches from activation by Cdc20 to Cdh1. *J. Cell Biol.* 157:1125–1137. <https://doi.org/10.1083/jcb.200111001>
- Heaney, A.P., G.A. Horwitz, Z. Wang, R. Singson, and S. Melmed. 1999. Early involvement of estrogen-induced pituitary tumor transforming gene and fibroblast growth factor expression in prolactinoma pathogenesis. *Nat. Med.* 5:1317–1321. <https://doi.org/10.1038/15275>
- Hellmuth, S., F. Böttger, C. Pan, M. Mann, and O. Stemmann. 2014. PP2A delays APC/C-dependent degradation of separase-associated but not free securin. *EMBO J.* 33:1134–1147. <https://doi.org/10.1002/embj.201488098>
- Hellmuth, S., C. Pöhlmann, A. Brown, F. Böttger, M. Sprinzl, and O. Stemmann. 2015a. Positive and negative regulation of vertebrate separase by Cdk1-cyclin B1 may explain why securin is dispensable. *J. Biol. Chem.* 290:8002–8010. <https://doi.org/10.1074/jbc.M114.615310>
- Hellmuth, S., S. Rata, A. Brown, S. Heidmann, B. Novak, and O. Stemmann. 2015b. Human chromosome segregation involves multi-layered

- regulation of separase by the peptidyl-prolyl-isomerase Pin1. *Mol. Cell.* 58:495–506. <https://doi.org/10.1016/j.molcel.2015.03.025>
- Herbert, M., M. Levasseur, H. Homer, K. Yallop, A. Murdoch, and A. McDougall. 2003. Homologue disjunction in mouse oocytes requires proteolysis of securin and cyclin B1. *Nat. Cell Biol.* 5:1023–1025. <https://doi.org/10.1038/ncb1062>
- Horner, V.L., and M.F. Wolfner. 2008. Transitioning from egg to embryo: Triggers and mechanisms of egg activation. *Dev. Dyn.* 237:527–544. <https://doi.org/10.1002/dvdy.21454>
- Hornig, N.C.D., P.P. Knowles, N.Q. McDonald, and F. Uhlmann. 2002. The dual mechanism of separase regulation by securin. *Curr. Biol.* 12: 973–982. [https://doi.org/10.1016/S0960-9822\(02\)00847-3](https://doi.org/10.1016/S0960-9822(02)00847-3)
- Howe, M., K.L. McDonald, D.G. Albertson, and B.J. Meyer. 2001. HIM-10 is required for kinetochore structure and function on *Caenorhabditis elegans* holocentric chromosomes. *J. Cell Biol.* 153:1227–1238. <https://doi.org/10.1083/jcb.153.6.1227>
- Howell, B.J., B.F. McEwen, J.C. Canman, D.B. Hoffman, E.M. Farrar, C.L. Rieder, and E.D. Salmon. 2001. Cytoplasmic dynein/dynactin drives kinetochore protein transport to the spindle poles and has a role in mitotic spindle checkpoint inactivation. *J. Cell Biol.* 155:1159–1172. <https://doi.org/10.1083/jcb.200105093>
- Jensen, S., M. Segal, D.J. Clarke, and S.I. Reed. 2001. A novel role of the budding yeast separin Esp1 in anaphase spindle elongation: Evidence that proper spindle association of Esp1 is regulated by Pds1. *J. Cell Biol.* 152:27–40. <https://doi.org/10.1083/jcb.152.1.27>
- Kamenz, J., T. Mihaljev, A. Kubis, S. Legewie, and S. Hauf. 2015. Robust ordering of anaphase events by adaptive thresholds and competing degradation pathways. *Mol. Cell.* 60:446–459. <https://doi.org/10.1016/j.molcel.2015.09.022>
- Kim, E., L. Sun, C.V. Gabel, and C. Fang-Yen. 2013. Long-term imaging of *Caenorhabditis elegans* using nanoparticle-mediated immobilization. *PLoS One.* 8:e53419. <https://doi.org/10.1371/journal.pone.0053419>
- Kimura, K., and A. Kimura. 2012. Rab6 is required for the exocytosis of cortical granules and the recruitment of separase to the granules during the oocyte-to-embryo transition in *Caenorhabditis elegans*. *J. Cell Sci.* 125:5897–5905. <https://doi.org/10.1242/jcs.116400>
- Kitagawa, R., E. Law, L. Tang, and A.M. Rose. 2002. The Cdc20 homolog, FZY-1, and its interacting protein, IFY-1, are required for proper chromosome segregation in *Caenorhabditis elegans*. *Curr. Biol.* 12:2118–2123. [https://doi.org/10.1016/S0960-9822\(02\)01392-1](https://doi.org/10.1016/S0960-9822(02)01392-1)
- Knight, A.J., N.M. Johnson, and C.A. Behm. 2012. VHA-19 is essential in *Caenorhabditis elegans* oocytes for embryogenesis and is involved in trafficking in oocytes. *PLoS One.* 7:e40317. <https://doi.org/10.1371/journal.pone.0040317>
- Leismann, O., A. Herzig, S. Heidmann, and C.F. Lehner. 2000. Degradation of *Drosophila* PIM regulates sister chromatid separation during mitosis. *Genes Dev.* 14:2192–2205. <https://doi.org/10.1101/gad.176700>
- Liu, M. 2011. The biology and dynamics of mammalian cortical granules. *Reprod. Biol. Endocrinol.* 9:149. <https://doi.org/10.1186/1477-7827-9-149>
- Liu, M., D. Sims, P. Calarco, and P. Talbot. 2003. Biochemical heterogeneity, migration, and pre-fertilization release of mouse oocyte cortical granules. *Reprod. Biol. Endocrinol.* 1:77. <https://doi.org/10.1186/1477-7827-1-77>
- Lu, D., J.Y. Hsiao, N.E. Davey, V.A. Van Voorhis, S.A. Foster, C. Tang, and D.O. Morgan. 2014. Multiple mechanisms determine the order of APC/C substrate degradation in mitosis. *J. Cell Biol.* 207:23–39. <https://doi.org/10.1083/jcb.201402041>
- Lui, D.Y., and M.P. Colaiácovo. 2013. Meiotic development in *Caenorhabditis elegans*. *Adv. Exp. Med. Biol.* 757:133–170. https://doi.org/10.1007/978-1-4614-4015-4_6
- MacKenzie, A., V. Vicory, and S. Lacefield. 2023. Meiotic cells escape prolonged spindle checkpoint activity through kinetochore silencing and slippage. *PLoS Genet.* 19:e1010707. <https://doi.org/10.1371/journal.pgen.1010707>
- McAinsh, A.D., and G.J.P.L. Kops. 2023. Principles and dynamics of spindle assembly checkpoint signalling. *Nat. Rev. Mol. Cell Biol.* 24:543–559. <https://doi.org/10.1038/s41580-023-00593-z>
- McCarter, J., B. Bartlett, T. Dang, and T. Schedl. 1999. On the control of oocyte meiotic maturation and ovulation in *Caenorhabditis elegans*. *Dev. Biol.* 205:111–128. <https://doi.org/10.1006/dbio.1998.9109>
- McNally, K.L., and F.J. McNally. 2005. Fertilization initiates the transition from anaphase I to metaphase II during female meiosis in *C. elegans*. *Dev. Biol.* 282:218–230. <https://doi.org/10.1016/j.ydbio.2005.03.009>
- McNally, K.P., E.A. Beath, B.M. Danlasky, C. Barroso, T. Gong, W. Li, E. Martinez-Perez, and F.J. McNally. 2022. Cohesin is required for meiotic spindle assembly independent of its role in cohesion in *C. elegans*. *PLoS Genet.* 18:e1010136. <https://doi.org/10.1371/journal.pgen.1010136>
- Merritt, C., D. Rasoloson, D. Ko, and G. Seydoux. 2008. 3' UTRs are the primary regulators of gene expression in the *C. elegans* germline. *Curr. Biol.* 18:1476–1482. <https://doi.org/10.1016/j.cub.2008.08.013>
- Meyer, R., V. Fofanov, A. Panigrahi, F. Merchant, N. Zhang, and D. Pati. 2009. Overexpression and mislocalization of the chromosomal segregation protein separase in multiple human cancers. *Clin. Cancer Res.* 15: 2703–2710. <https://doi.org/10.1158/1078-0432.CCR-08-2454>
- Mitchell, D.M., L.R. Uehlein-Klebanow, and J.N. Bembeneck. 2014. Protease-dead separase is dominant negative in the *C. elegans* embryo. *PLoS One.* 9:e108188. <https://doi.org/10.1371/journal.pone.0108188>
- Mogessie, B., K. Scheffler, and M. Schuh. 2018. Assembly and positioning of the oocyte meiotic spindle. *Annu. Rev. Cell Dev. Biol.* 34:381–403. <https://doi.org/10.1146/annurev-cellbio-100616-060553>
- Monen, J., N. Hattersley, A. Muroyama, D. Stevens, K. Oegema, and A. Desai. 2015. Separase cleaves the N-tail of the CENP-A related protein CPAR-1 at the meiosis I metaphase-anaphase transition in *C. elegans*. *PLoS One.* 10:e0125382. <https://doi.org/10.1371/journal.pone.0125382>
- Monen, J., P.S. Maddox, F. Hyndman, K. Oegema, and A. Desai. 2005. Differential role of CENP-A in the segregation of holocentric *C. elegans* chromosomes during meiosis and mitosis. *Nat. Cell Biol.* 7:1248–1255. <https://doi.org/10.1038/ncb1331>
- Moschou, P.N., A.P. Smertenko, E.A. Minina, K. Fukada, E.I. Savenkov, S. Robert, P.J. Hussey, and P.V. Bozhkov. 2013. The caspase-related protease separase (extra spindle poles) regulates cell polarity and cytokinesis in *Arabidopsis*. *Plant Cell.* 25:2171–2186. <https://doi.org/10.1105/tpc.113.113043>
- Musacchio, A. 2015. The molecular biology of spindle assembly checkpoint signaling dynamics. *Curr. Biol.* 25:R1002–R1018. <https://doi.org/10.1016/j.cub.2015.08.051>
- Muscat, C.C., K.M. Torre-Santiago, M.V. Tran, J.A. Powers, and S.M. Wignall. 2015. Kinetochore-independent chromosome segregation driven by lateral microtubule bundles. *Elife.* 4:e06462. <https://doi.org/10.7554/eLife.06462>
- Nam, H.-J., and J.M. van Deursen. 2014. Cyclin B2 and p53 control proper timing of centrosome separation. *Nat. Cell Biol.* 16:538–549. <https://doi.org/10.1038/ncb2952>
- Olson, S.K., G. Greenan, A. Desai, T. Müller-Reichert, and K. Oegema. 2012. Hierarchical assembly of the eggshell and permeability barrier in *C. elegans*. *J. Cell Biol.* 198:731–748. <https://doi.org/10.1083/jcb.201206008>
- Paix, A., A. Folkmann, D. Rasoloson, and G. Seydoux. 2015. High efficiency, homology-directed genome editing in *Caenorhabditis elegans* using CRISPR-Cas9 ribonucleoprotein complexes. *Genetics.* 201:47–54. <https://doi.org/10.1534/genetics.115.179382>
- Praitis, V., E. Casey, D. Collar, and J. Austin. 2001. Creation of low-copy integrated transgenic lines in *Caenorhabditis elegans*. *Genetics.* 157: 1217–1226. <https://doi.org/10.1093/genetics/157.3.1217>
- Quiogue, A.R., E. Sumiyoshi, A. Fries, C.-H. Chuang, and B. Bowerman. 2023. Microtubules oppose cortical actomyosin-driven membrane ingression during *C. elegans* meiosis I polar body extrusion. *PLoS Genet.* 19: e1010984. <https://doi.org/10.1371/journal.pgen.1010984>
- Richie, C.T., J.N. Bembeneck, B. Chestnut, T. Furuta, J.M. Schumacher, M. Wallenfang, and A. Golden. 2011. Protein phosphatase 5 is a negative regulator of separase function during cortical granule exocytosis in *C. elegans*. *J. Cell Sci.* 124:2903–2913. <https://doi.org/10.1242/jcs.073379>
- Rosen, L.E., J.E. Klebba, J.B. Asfaha, C.M. Ghent, M.G. Campbell, Y. Cheng, and D.O. Morgan. 2019. Cohesin cleavage by separase is enhanced by a substrate motif distinct from the cleavage site. *Nat. Commun.* 10:5189. <https://doi.org/10.1038/s41467-019-13209-y>
- Sato, M., B.D. Grant, A. Harada, and K. Sato. 2008. Rab11 is required for synchronous secretion of chondroitin proteoglycans after fertilization in *Caenorhabditis elegans*. *J. Cell Sci.* 121:3177–3186. <https://doi.org/10.1242/jcs.034678>
- Schwarzstein, M., S.M. Wignall, and A.M. Villeneuve. 2010. Coordinating cohesion, co-orientation, and congression during meiosis: Lessons from holocentric chromosomes. *Genes Dev.* 24:219–228. <https://doi.org/10.1101/gad.1863610>
- Severson, A.F., and B.J. Meyer. 2014. Divergent kleisin subunits of cohesin specify mechanisms to tether and release meiotic chromosomes. *Elife.* 3: e03467. <https://doi.org/10.7554/eLife.03467>
- Shindo, N., K. Kumada, and T. Hirota. 2012. Separase sensor reveals dual roles for separase coordinating cohesin cleavage and cdk1 inhibition. *Dev. Cell.* 23:112–123. <https://doi.org/10.1016/j.devcel.2012.06.015>

- Stein, K.K., and A. Golden. 2018. The *C. elegans* eggshell. *WormBook*. 2018: 1–36. <https://doi.org/10.1895/wormbook.1.179.1>
- Stemmann, O., H. Zou, S.A. Gerber, S.P. Gygi, and M.W. Kirschner. 2001. Dual inhibition of sister chromatid separation at metaphase. *Cell*. 107: 715–726. [https://doi.org/10.1016/S0092-8674\(01\)00603-1](https://doi.org/10.1016/S0092-8674(01)00603-1)
- Sun, Y., M. Kucej, H.-Y. Fan, H. Yu, Q.-Y. Sun, and H. Zou. 2009. Separase is recruited to mitotic chromosomes to dissolve sister chromatid cohesion in a DNA-dependent manner. *Cell*. 137:123–132. <https://doi.org/10.1016/j.cell.2009.01.040>
- Thomas, C., B. Wetherall, M.D. Levasseur, R.J. Harris, S.T. Kerridge, J.M.G. Higgins, O.R. Davies, and S. Madgwick. 2021. A prometaphase mechanism of securin destruction is essential for meiotic progression in mouse oocytes. *Nat. Commun.* 12:4322. <https://doi.org/10.1038/s41467-021-24554-2>
- Tsou, M.-F.B., W.-J. Wang, K.A. George, K. Uryu, T. Stearns, and P.V. Jallepalli. 2009. Polo kinase and separase regulate the mitotic licensing of centriole duplication in human cells. *Dev. Cell*. 17:344–354. <https://doi.org/10.1016/j.devcel.2009.07.015>
- Tunquist, B.J., and J.L. Maller. 2003. Under arrest: Cytostatic factor (CSF)-mediated metaphase arrest in vertebrate eggs. *Genes Dev.* 17:683–710. <https://doi.org/10.1101/gad.1071303>
- Uhlmann, F., D. Wernic, M.-A. Poupard, E.V. Koonin, and K. Nasmyth. 2000. Cleavage of cohesin by the CD clan protease separin triggers anaphase in yeast. *Cell*. 103:375–386. [https://doi.org/10.1016/S0092-8674\(00\)00130-6](https://doi.org/10.1016/S0092-8674(00)00130-6)
- Viadiu, H., O. Stemmann, M.W. Kirschner, and T. Walz. 2005. Domain structure of separase and its binding to securin as determined by EM. *Nat. Struct. Mol. Biol.* 12:552–553. <https://doi.org/10.1038/nsmb935>
- Waizenegger, I., J.F. Giménez-Abián, D. Wernic, and J.-M. Peters. 2002. Regulation of human separase by securin binding and autocleavage. *Curr. Biol.* 12:1368–1378. [https://doi.org/10.1016/S0960-9822\(02\)01073-4](https://doi.org/10.1016/S0960-9822(02)01073-4)
- Wang, R., Z. Kaul, C. Ambardekar, T.G. Yamamoto, K. Kavdia, K. Kodali, A.A. High, and R. Kitagawa. 2013. HECT-E3 ligase ETC-1 regulates securin and cyclin B1 cytoplasmic abundance to promote timely anaphase during meiosis in *C. elegans*. *Development*. 140:2149–2159. <https://doi.org/10.1242/dev.090688>
- Watson, E.R., N.G. Brown, J.-M. Peters, H. Stark, and B.A. Schulman. 2019. Posing the APC/C E3 ubiquitin ligase to orchestrate cell division. *Trends Cell Biol.* 29:117–134. <https://doi.org/10.1016/j.tcb.2018.09.007>
- Weber, J., Z. Kabakci, S. Chaurasia, E. Brunner, and C.F. Lehner. 2020. Chromosome separation during *Drosophila* male meiosis I requires separase-mediated cleavage of the homolog conjunction protein UNO. *PLoS Genet.* 16:e1008928. <https://doi.org/10.1371/journal.pgen.1008928>
- Wessel, G.M., J.M. Brooks, E. Green, S. Haley, E. Voronina, J. Wong, V. Zaydfudim, and S. Conner. 2001. The biology of cortical granules. *Int. Rev. Cytol.* 209:117–206. [https://doi.org/10.1016/S0074-7696\(01\)09012-X](https://doi.org/10.1016/S0074-7696(01)09012-X)
- Yaakov, G., K. Thorn, and D.O. Morgan. 2012. Separase biosensor reveals that cohesin cleavage timing depends on phosphatase PP2A(Cdc55) regulation. *Dev. Cell*. 23:124–136. <https://doi.org/10.1016/j.devcel.2012.06.007>
- Yamamoto, T.G., S. Watanabe, A. Essex, and R. Kitagawa. 2008. SPDL-1 functions as a kinetochore receptor for MDF-1 in *Caenorhabditis elegans*. *J. Cell Biol.* 183:187–194. <https://doi.org/10.1083/jcb.200805185>
- Yang, H.Y., P.E. Mains, and F.J. McNally. 2005. Kinesin-1 mediates translocation of the meiotic spindle to the oocyte cortex through KCA-1, a novel cargo adapter. *J. Cell Biol.* 169:447–457. <https://doi.org/10.1083/jcb.200411132>
- Yang, H.Y., K. McNally, and F.J. McNally. 2003. MEI-1/katanin is required for translocation of the meiosis I spindle to the oocyte cortex in *C. elegans*. *Dev. Biol.* 260:245–259. [https://doi.org/10.1016/S0012-1606\(03\)00216-1](https://doi.org/10.1016/S0012-1606(03)00216-1)
- Yu, J., P. Raia, C.M. Ghent, T. Raisch, Y. Sadian, S. Cavadini, P.M. Sabale, D. Barford, S. Raunser, D.O. Morgan, and A. Boland. 2021. Structural basis of human separase regulation by securin and CDK1-cyclin B1. *Nature*. 596:138–142. <https://doi.org/10.1038/s41586-021-03764-0>
- Yu, R., S.-G. Ren, G.A. Horwitz, Z. Wang, and S. Melmed. 2000. Pituitary tumor transforming gene (PTTG) regulates placental JEG-3 cell division and survival: Evidence from live cell imaging. *Mol. Endocrinol.* 14: 1137–1146. <https://doi.org/10.1210/mend.14.8.0501>
- Zur, A., and M. Brandeis. 2001. Securin degradation is mediated by fzy and fzr, and is required for complete chromatid separation but not for cytokinesis. *EMBO J.* 20:792–801. <https://doi.org/10.1093/emboj/20.4.792>

Supplemental material

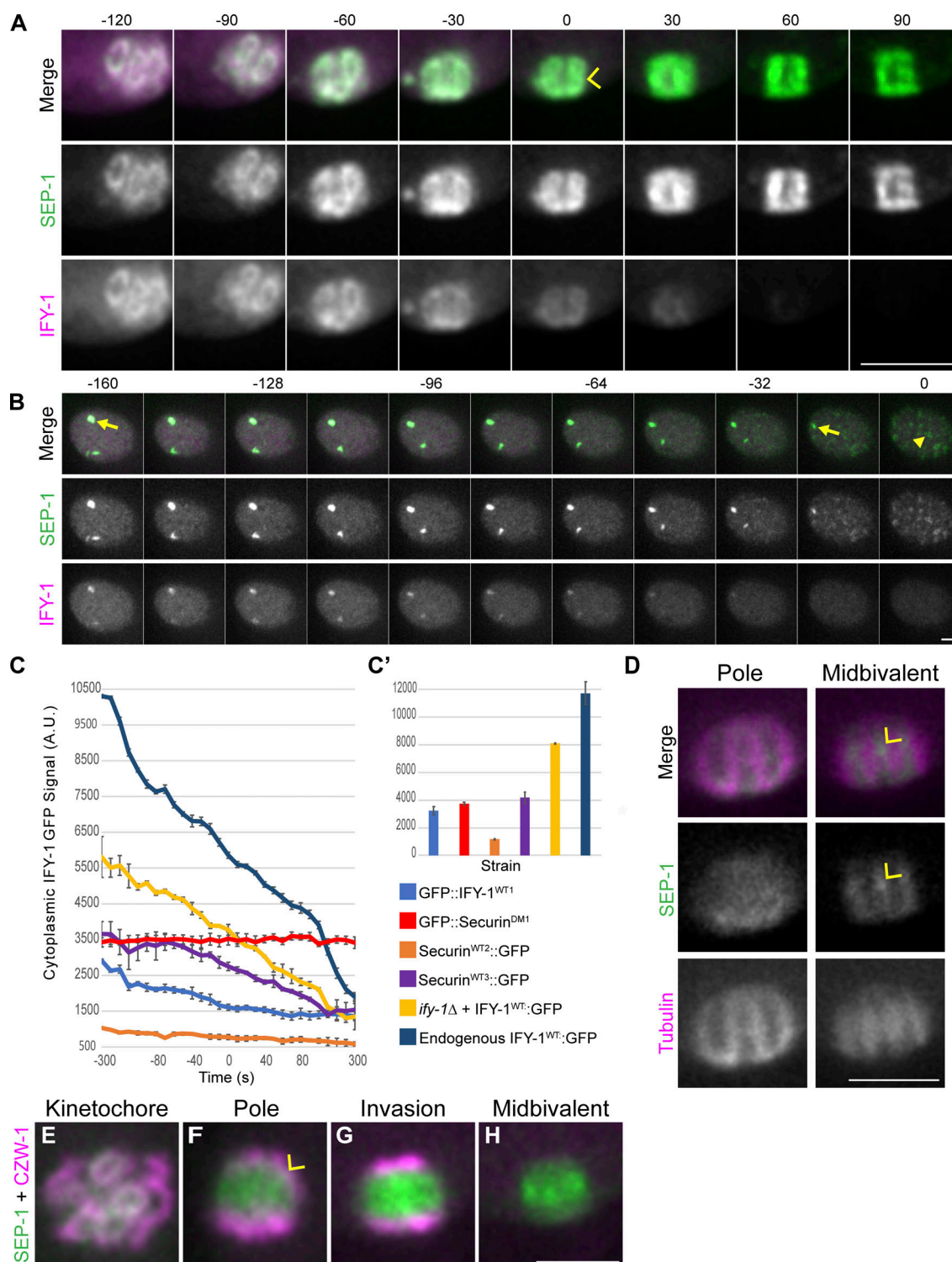


Figure S1. Dynamics of separase and securin during meiosis I. (A) Endogenously tagged SEP-1::mScarlet (green) and IFY-1::GFP (magenta) colocalize on the spindle at the metaphase to anaphase transition. Securin is rapidly degraded while separase relocates to the midbivalent (yellow caret) at anaphase onset (time shown in seconds, $t = 0$ is anaphase onset). (B) Cortical images of SEP-1::mScarlet (magenta) and IFY-1::GFP (green). IFY-1::GFP colocalizes with SEP-1::mScarlet on linear elements (yellow arrow) until it is degraded before separase relocates to vesicles (time shown in seconds, $t = 0$ marks vesicle localization). (C) Quantification of cytoplasmic securin levels in different WT or mutant securin GFP lines ($t = 0$ denotes anaphase onset). (C') Cytoplasmic GFP levels measured in embryos 300 s before anaphase showing similar expression in WT1 and DM1 lines used throughout the manuscript. (D) Images of endogenously tagged SEP-1::mScarlet (green) and Tubulin::mCherry (magenta) show polar enriched separase within the tubulin cage and midbivalent separase (yellow caret) between microtubule bundles. (E–H) Endogenously tagged SEP-1::mScarlet (green) colocalizes with CZW-1::GFP (magenta, Yamamoto et al., 2008) at kinetochores during prometaphase I, partially colocalizes with CZW-1::GFP at the spindle pole (yellow caret) before midbivalent localization in anaphase. Scale bars: 5 μ m.

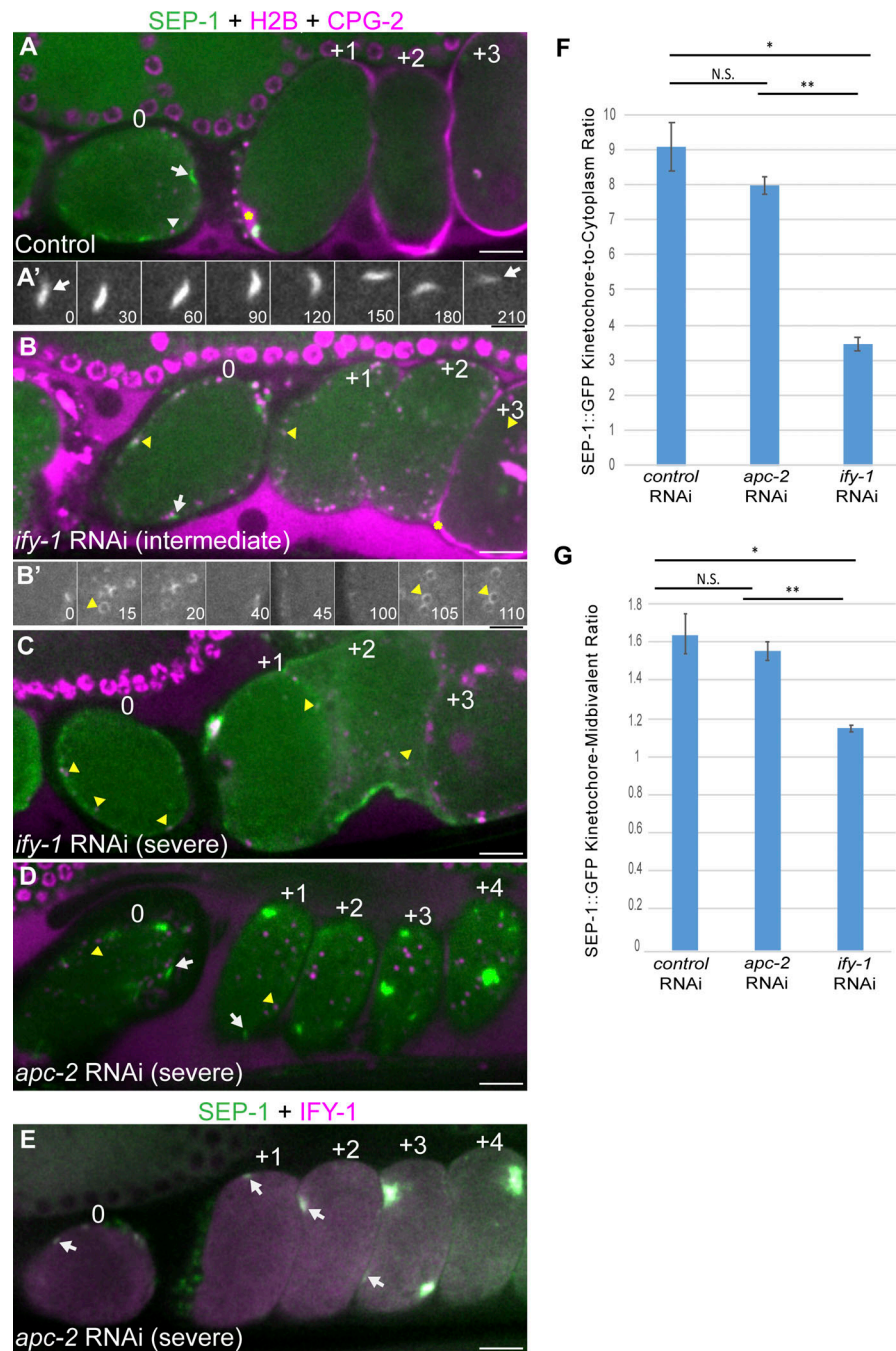


Figure S2. Regulation of separase localization. (A–D) Germline images of worms expressing endogenously tagged SEP-1::GFP (green), H2B::mCherry, and mCherry::CPG-2 (magenta). Numbers indicate embryo position in the uterus, corresponding to increasing age. (A and A') In control animals, prometaphase I embryos in the spermatheca (embryo 0) have mCherry::CPG-2 in vesicles (white arrowhead), while older embryos (+1–+3) have mCherry::CPG-2 in the eggshell (yellow asterisk). SEP-1::GFP localizes to linear elements (white arrow). (A') Montage of a time series of a prometaphase I oocyte/embryo from ovulation ($t = 0$) shows SEP-1::GFP localized to linear elements (white arrows). (B) Intermediate *ify-1*(RNAi) embryos in the spermatheca (0), and multiple older embryos (+1–+2) have SEP-1::GFP abnormally localized to cortical granules (yellow arrowheads). Eventually, mCherry::CPG-2 signal appears in the eggshell of older embryos (+3, asterisk), suggesting delayed and reduced secretion. (B') Montage of a prometaphase *ify-1*(RNAi) oocyte/embryo beginning at ovulation shows premature SEP-1::GFP localized to cortical granules (yellow arrowheads). (C) Severe *ifv-1*(RNAi) prometaphase I embryos in the spermatheca (0) and multiple older embryos (+1–+2) have SEP-1::GFP abnormally localized to cortical granules (yellow arrowheads), while mCherry::CPG-2 signal does not accumulate in the eggshell. (D) In *apc-2*(RNAi) embryos in the spermatheca (embryo 0) and numerous arrested embryos, SEP-1::GFP remains localized to linear elements (arrow) but not vesicles (arrowhead), with mCherry::CPG-2 remaining in cortical granules (yellow arrowheads). (E) SEP-1::mScarlet (green) colocalizes with IFY-1::GFP (magenta) on linear elements (white arrows) in multiple embryos after *apc-2* RNAi. (F) Quantification of SEP-1::GFP associated with kinetochores during prometaphase I after control ($N = 5$), *apc-2* ($N = 5$), or *ify-1* ($N = 13$) RNAi. (G) Quantification of SEP-1::GFP signal on the kinetochore relative to the midbivalent region in prometaphase I after control ($n = 15$), *apc-2* ($n = 19$), or *ify-1* ($n = 8$) RNAi. Asterisks denote a statistically significant difference, P value $< 1 \times 10^{-6}$. N = spindles scored, n = optimal side-view images of homologs scored. For montages (A' and B') time is in seconds, $t = 0$ is ovulation. Scale bars: 10 μ m in all except A' and B', which are 5 μ m.

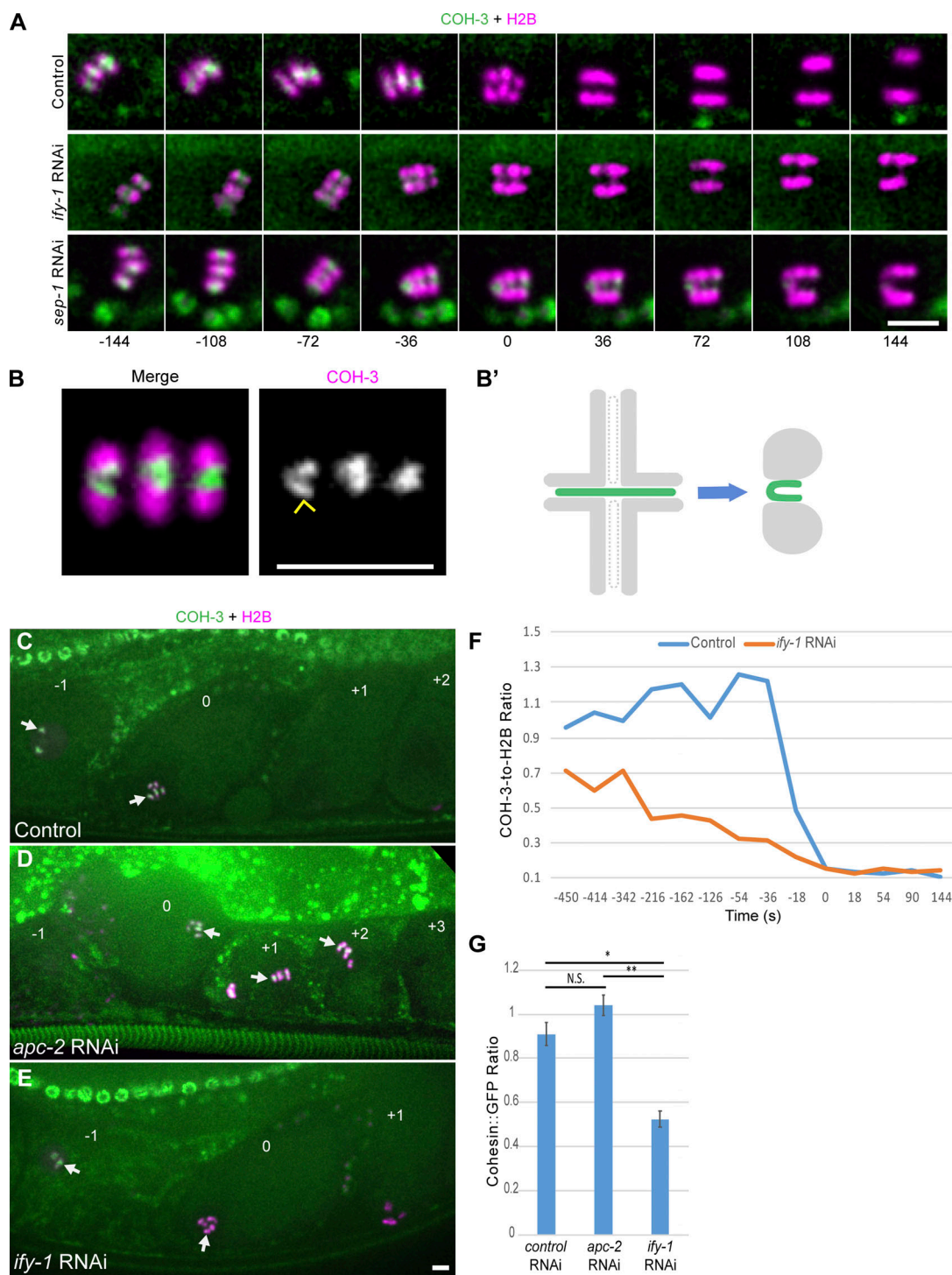


Figure S3. Meiosis I cohesin dynamics and regulation during meiosis I. (A) Kymographs of anaphase onset in embryos expressing GFP::COH-3 (green) and H2B::mCherry (magenta). Time (s) is relative to anaphase I onset ($t = 0$). GFP::COH-3 remains high until seconds before anaphase I onset in WT, is reduced before anaphase onset in *ify-1(RNAi)* embryos, and persists past anaphase I in *sep-1(RNAi)* embryos. (B) Representative image of GFP::COH-3 (green) and H2B::mCherry (magenta) showing a folded short arm (yellow caret) from different orientations on three bivalents. (B') Proposed model of GFP::COH-3 at the bivalent short arm adopting a folded configuration based on images from 10 embryos at several stages of meiosis I. (C) In control, GFP::COH-3 midbivalent signal is similar in oocytes (-1) and prometaphase I embryos (labeled 0, white arrows) but is absent from embryos after meiosis I in the uterus (+1, +2). (D) After *apc-2 RNAi*, GFP::COH-3 levels are retained at the midbivalent in prometaphase I embryos (0) and several arrested embryos in the uterus (+1, +2). (E) GFP::COH-3 midbivalent signal is prematurely reduced after *ify-1 RNAi*, in prometaphase I embryos (labeled 0) relative to oocytes (-1) and is not observed in older embryos (+1). (F) Quantification of GFP::COH-3 levels relative to H2B from a time series of control or *ify-1(RNAi)* embryos. Time (s) is relative to anaphase I onset. (G) Quantification of the ratio between the GFP::COH-3 signal at the midbivalent in prometaphase I embryo relative to the -1 oocyte in the same plane. The GFP::COH-3 signal ratio was near 1 in control ($N = 10$) and *apc-2 RNAi* ($N = 5$, $P > 0.05$) but was significantly reduced (about 50% reduction) after *ify-1 RNAi* ($N = 13$, $P < 0.05$). Scale bars: 5 μm .

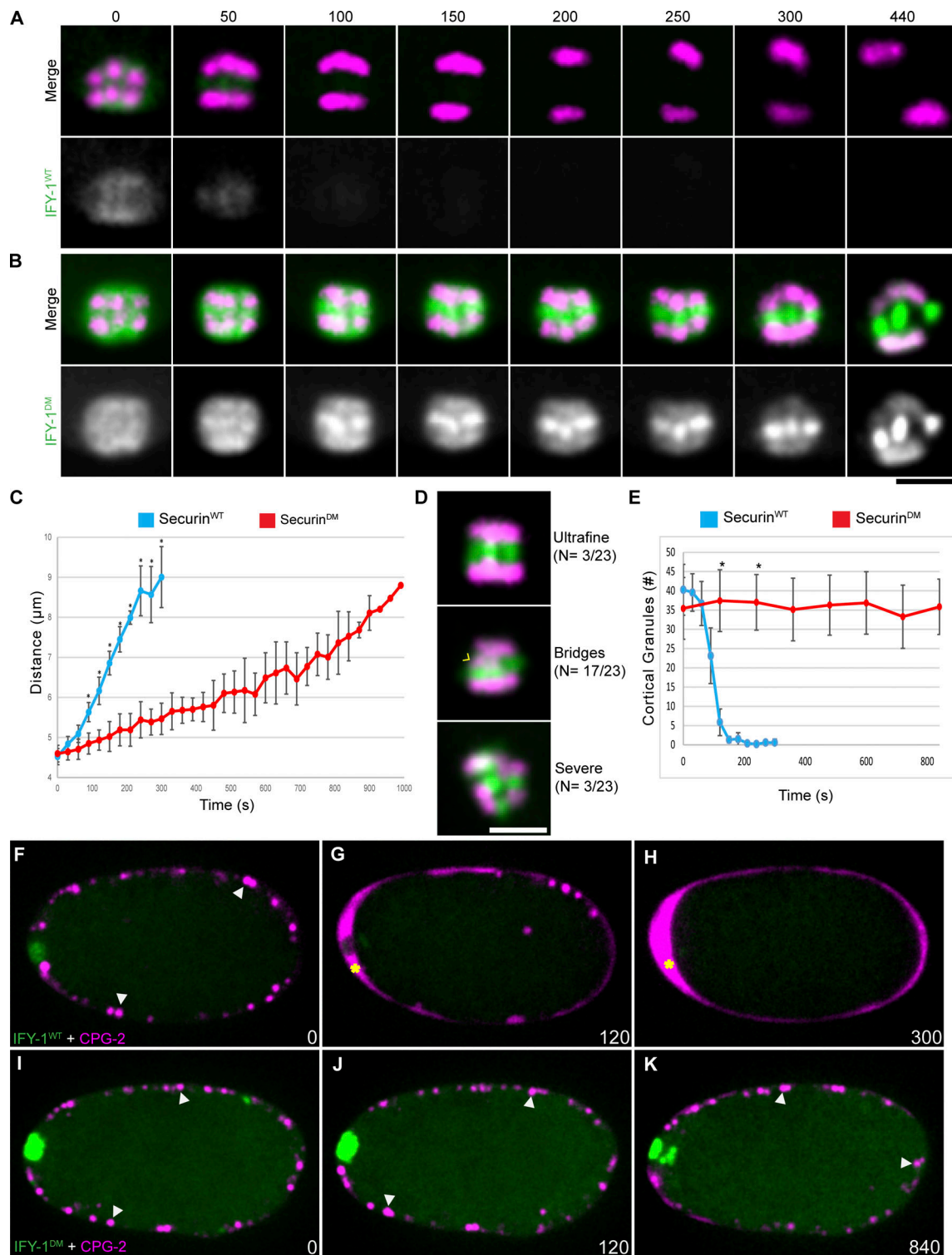


Figure S4. GFP::IFY-1^{DM} inhibits chromosome segregation and exocytosis. (A) GFP::IFY-1^{WT} or (B) GFP::IFY-1^{DM} (green) with H2B::mCherry (magenta) during meiosis I. Chromosomes move apart quickly in GFP::IFY-1^{WT} but are severely delayed in GFP::IFY-1^{DM} embryos. Time (s) is relative to anaphase onset. (C) Average distance between chromosomes during anaphase I is significantly reduced in IFY-1^{DM}:GFP embryos relative to control (N = 9 for GFP::IFY-1^{WT}, N > 18 for GFP::IFY-1^{DM}, asterisks denote a statistically significant difference, P value = <0.05). (D) Frequency and images of chromosome segregation defects (yellow caret) observed in embryos expressing GFP::IFY-1^{DM} (green, H2B::mCherry in magenta). N = number of embryos scored. (E–K) GFP::IFY-1^{DM} blocks cortical granule exocytosis. (E) Quantification of cortical granules in a single spindle plane over time after anaphase I onset (N = 6 for GFP::IFY-1^{WT}, N = 7 for GFP::IFY-1^{DM}). Asterisks denote a statistically significant difference, P value <0.0001. Error bars represent standard error of the mean. (F–H) Images shown of GFP::IFY-1^{WT} or (I–K) GFP::IFY-1^{DM} (green) and mCherry::CPG-2 (magenta, arrowheads) during meiosis I. Time (seconds) is relative to midbivalent localization. In wildtype, most vesicles (arrowheads) undergo exocytosis after 120 s of anaphase onset (G) while mCherry::CPG-2 is extracellular (H, yellow asterisk). (I–K) In contrast, cortical granules (arrowheads) are retained in GFP::IFY-1^{DM} embryos, even after several minutes. Scalebar: 5 μm (A, B, and D), 10 μm (F–K).

Video 1. **Chromosome dynamics at the metaphase-to-anaphase transition of meiosis I.** Single plane time-lapse image series of embryos expressing H2B::mCherry with SEP-1::GFP, COH-3::GFP, GFP::IFY-1^{WT}, or GFP::IFY-1^{DM}. mCherry is shown in magenta and GFP is shown in green. Time (seconds) is normalized to anaphase I onset ($t = 0$). The playback speed is seven frames per second.

Video 2. **Separase dynamics at anaphase onset of meiosis I.** Single-plane movies of embryos expressing SEP-1 (shown in green) with H2B, COH-3, or IFY-1^{WT} (shown in magenta). Time (seconds) is normalized to anaphase I onset ($t = 0$). The playback speed is seven frames per second.

Video 3. **Securin and separase dynamics in the cortex during anaphase I.** Cortical time series from worms expressing SEP-1 (shown in green) with IFY-1 or RAB-11 (shown in magenta). Time (s) is normalized to anaphase I onset ($t = 0$). The SEP-1 + IFY-1 movie is a max projection acquired with a 60× objective, while SEP-1 + RAB-11 is a single-plane movie acquired with a 100× objective. Playback speed is seven frames per second.

Video 4. **GFP::IFY-1^{DM} blocks cortical granule exocytosis during meiosis I.** Single plane time-lapse image series of embryos expressing CPG-2::mCherry (magenta) with GFP::IFY-1^{WT} or GFP::IFY-1^{DM} (green). Time (seconds) is normalized to anaphase I onset ($t = 0$). The playback speed is seven frames per second.

Video 5. **GFP::IFY-1^{DM} does not affect separase relocation to the midbivalent in anaphase I.** Single plane time lapse image series of embryos expressing SEP-1 (green) with GFP::IFY-1^{WT} or GFP::IFY-1^{DM} (magenta). Time (seconds) is normalized to anaphase I onset ($t = 0$). The playback speed is five frames per second.

Video 6. **GFP::IFY-1^{DM} prevents cortical granule localization of separase during anaphase I.** Cortical max projections from a time-lapse image series of embryos expressing SEP-1 (green) and CAV-1 (magenta) with GFP::IFY-1^{WT} or GFP::IFY-1^{DM} (magenta). Time (seconds) is normalized to anaphase I onset ($t = 0$). The playback speed is three frames per second.

Provided online is Table S1. Table S1 lists *C. elegans* strains used in this study.